國 立 交 通 大 學

材料科學與工程學系

博 士 論 文

層狀矽酸鹽補強聚丙烯晴-丁二烯橡膠與聚丁二烯橡膠奈米複合材料之性質研究

Mechanical and Morphological Effects of Layered silicates on Nitrile-Butadiene and Butadiene Rubber Nanocomposites

研究生： 黃為國 (Wei-Gwo Hwang)

指導教授： 韋光華 (Kung-Hwa Wei)

中華民國 九十四 年 十二 月

層狀矽酸鹽補強聚丙烯晴-丁二烯橡膠與聚丁二烯橡膠奈米複合材料之性質研究

Mechanical and Morphological Effects of Layered silicates on Nitrile-Butadiene and Butadiene Rubber Nanocomposites

研 究 生：黃為國　　　Student：Wei-Gwo Hwang

指 導 教 授：韋光華　　　Advisor：Kung-Hwa Wei

國 立 交 通 大 學

材 料 科 學 與 工 程 系

博 士 論 文

A Thesis

Submitted to Department of Materials Science and Engineering

College of Engineering

National Chiao Tung University

in partial Fulfillment of the Requirements

for the Degree of

Doctor of Philosophy

in

Materials Science and Engineering

Oct 2005

Hsinchu, Taiwan, Republic of China

中華民國九十四年十二月

Abstract

In this thesis, a variety of methods are used to prepare the elastomer nanocomposites comprised of inorganic or organo-modified layered silicates and rubber matrices.   Excellent mechanical , thermal and barrier properties can be obtained for each nanocomposite by performing proper process design, material selection, physical and/or chemical reactions by the addition of compatibilizers or surfactants, etc.

In chapter 2, elastomer nanocomposites consisting of nitrile butadiene rubber (NBR) latex and layered silicates are prepared by a modified latex shear blending process aided with ball milling.   The mode of dispersion of layered silicates in NBR is partially exfoliated and intercalated when the concentration of layered silicates is below 7.5 wt %, as evidenced by transmission electron microscopy and X-ray diffraction results.   The tensile and tear properties are much higher than that of neat NBR.   Specifically, the tensile and tear mechanical properties of the NBR / layered silicates can increase by 200% and 60%, respectively.   The decomposition temperature of the nanocomposites increases slightly.

Different methods to form the nanocomposites of intercalated and exfoliated organosilicates in acrylonitrile butadiene rubber (NBR) are carried out by a solution blending process in chapter 3.   The dispersion and intergallery spacings of organosilicates in these nanocomposites are examined by transmission electron microscopy and X-ray diffraction.   Dramatic enhancements in the mechanical and thermal properties of NBR are found by incorporating less than ten parts of organosilicates.   The fluid impermeability is also improved significantly.

Nanocomposites of intercalated and exfoliated organosilicates in butadiene rubber (BR) have also been prepared by using a two-stage melt blending process in

chapter 4.   X-ray diffraction and transmission electron microscopy are used to examine, respectively, the intergallery spacing of the organosilicates and their dispersion in the BR.   Dramatic enhancements in the mechanical and thermal properties of BR occur when it incorporates less than 10 parts of organosilicates and the loading ratio of the organosilicate to dicarboxylic acid-terminated butadiene oligomer is about 3.   In addition, the relative water vapor permeability of the BR nanocomposites containing 10 parts of organosilicate—both in the presence and absence of the compatibilizer—reduce largely compared to that of the neat BR.

It can be concluded that the successfully prepared NBR(BR)/organosilicate nanocomposites having intercalated and partially exfoliated structures can be obtained by different blending methods in proper process design and material selection.   As a result of significantly improved compatibility and the strong molecular chains interactions between layered silicates and rubber matrices, the mechanical, thermal, and many other properties of these nanocomposites containing a low weight percent of layered silicates can be increased substantially.

摘要

本論文主旨為探討利用不同組成之有機或無機層狀矽酸鹽黏土強化橡膠材料所形成之奈米橡膠複材的性能改變結果，研究顯示經由適當之製程設計、材料選配與利用可產生化學或物理反應之界面活性劑、共溶劑等寡分子體之導入效果，可獲得極佳之機械性能改良，熱性能與阻斷性能(barrier property)提昇等。

本文第二章，探討利用乳化相摻混程序，並結合高剪力摻合及球磨分散方式可將無機層狀矽酸鹽黏土均勻混入 NBR 橡膠乳膠中，經由 X 光繞射檢測及 TEM 觀察結果顯示，當層狀矽酸鹽黏土含量低於 7.5 wt %時，可形成分散良好之部分剝層與插層結構之奈米橡膠複材，其機械性能如拉力與抗撕裂強度均比 NBR 原材料性能提昇相當多，分別提昇逾 200%與 60%，此外其熱分解溫度也相對提昇。

在第三章中，探討以溶液摻合作業方式製備有機改質之層狀矽酸鹽補強 NBR 橡膠所形成之奈米橡膠複材，經由 X 光繞射檢測及 TEM 觀察結果顯示，此一複材之結構為大部分插層與局部剝層之分散相，只需添加少於 10 份矽酸鹽黏土，即可製備具相當高強度與熱性質之奈米橡膠複材，其抗水滲透等性能也有顯著提昇。

在第四章中，探討經由二階段熔融摻合作業方式製備有機改質之層狀矽酸鹽補強 BR 橡膠所形成之奈米橡膠複材，經由 X 光繞射檢測及 TEM 觀察結果顯示，其結構為大部分插層之分散相，審慎選用有機黏土與共容劑，在含量少於 10 份之有機矽酸鹽黏土與約 3 份之共容劑可獲得最佳之機械與物理性能提昇，且抗水滲透等性能也有相對提昇。

本論文的研究結果可得到以下結論，經由適當之製程設計、材料選配，可以有許多不同途徑用以產製具有大部分插層與局部剝層型態學之奈米橡膠複材，

這主要是基於經有機改質或特殊表面處理的橡膠高分子與矽酸鹽補強材料之間所產生很強的分子間作用引力，與改善界面相容性之效果所致。

誌謝

Table of Content

Figure Lists

Chapter 1: Introduction

Chapter 2: Preparation and Mechanical Properties of Nitrile Butadiene Rubber/Silicate Nanocomposites

Chapter 3: Mechanical, Thermal, and Barrier Properties of

   NBR/Organosilicate Nanocomposites

Chapter 4: Synergistic Effect of Compatibilizer in Organo-modified

   Layered Silicate Reinforced BR Nanocomposites

Scheme & Table Lists

Chapter 1: Introduction

Chapter 2: Preparation and Mechanical Properties of Nitrile Butadiene Rubber/Silicate Nanocomposites

Chapter 3: Mechanical, Thermal, and Barrier Properties of NBR/Organosilicate Nanocomposites

Chapter 4: Synergistic Effect of Compatibilizer in Organo-modified Layered Silicate Reinforced BR Nanocomposites

Chapter 1: Introduction

1-1   Reinforcement of Nanoparticles

Nanocomposites are a new class of materials that comprise a dispersion of at least one dimension with nanometer-size particles classified as lamellar, fibrillar, shell-like, spherical and others in a matrix with single or multi-component.   Three types of nanocomposites are acknowledged dopending on the dimension numbers of the dispersed particles being in nanometer range.   Isodimensional nanoparticles are the first type which have three dimensions being in the order of of nanometers, such as spherical silica obtained by in-situ sol-gel methods [1-2] or by (living free radical) polymerization promoted directed from their surface [3-4].   In general, the interactions between the polymer and the silanol groups would generate during the sol-gel process, a macrophase separation should be avoided, and the resulted materials would have a high degree of homogeneity and optical transparency.   However, these properties are highly dependent on the reaction condition of the sol-gel process, e.g. the pH value.   The second type, an elongated structure formed by two dimensions being in nanometer scale and one dimension being larger are nanotubes or whiskers, such as carbon nanotubes.   The third type of nanocomposites is characterized by only one dimension in the nanometer range, usually named as polymer/layered silicate nanocomposites, where the filler is present in the form of sheets of one to several nanometers thick and hundreds to thousands nanometers long.

On recent developments, polymer/layered silicate nanocomposites have attracted the attention of government, academic, and industrial researchers [5-11].   This new type of composites, based on nanometer range of organic or inorganic clays dispersed in a variety of polymer matrices, i.e. thermoplastics, thermosets, resins, and

elastomers, prepared via various synthetic routes, including in-situ intercalative polymerization, exfoliation-adsorption (from polymers or prepolymers in solution, emulsion polymerization), template synthesis, and melt intercalation.   The highly enhanced mechanical and thermal properties of the new class polymer nanocomposites are usually reinforced by only small amount (e. g. lower than 10 weight percentage) of nanoscopically dispersed intercalated and/or exfoliated layered silicates relative to the unfilled polymer.   Once the nanolayer exfoliation has been achieved, these remarkably improved properties of the nanocomposites can be manifested, including tensile strength, modulus or stiffness, heat distortion temperature, flame retardance, barrier properties, and so forth, which result from the special structure and morphology of these nanocomposites with respective to conventional composites [12].

Among several reinforcements and fillers, carbon black is the most important reinforcing agent used in elastomeric industry.   It produces a remarkable reinforcing effect on vulcanized rubber because it has a variety of active functional groups such as carboxyl, phenolic, and quinine groups on the surface of the particles that leads to strong interaction with the rubber chains.   However, carbon black causes pollution, gives black color, increases the compound viscosity and impairs the processibility of the compound when it is incorporated in a large amount into rubber.   Many light or pale color reinforcing agents, such as kaolin, precipitated silica, and sepiolite, etc. were researched to replace carbon black.   Nevertheless, their reinforcing properties are lower than those of carbon black because of their hydrophilic nature which leads to poor compatibility and decreases the intermolecular force between those fillers and polymer matrices.   Conventional polymer/clay composites containing aggregated and non-homogeneous nanolayer tactoids ordinarily can improve rigidity, but they often sacrifice elongation, toughness, and strength.

The complete dispersion of clay nanolayers, also termed as layered silicates, with the single layered silicate or bundles reduced in size from 100 microns to several nanometers is called as exfoliation in a polymer matrix. The structure of polymer/layered silicate nanocomposite would optimize the chain reaction cites (e.g. high aspect ratio and the whole surface area effect) of layered silicates and confine the polymer molecules to isolate and force them into an orderly arrangement in these two-dimensional spaces, which, in turn, results in significant improvement of the combined physical and mechanical properties of the polymer nanocomposite. Depending on the nature of the components used (layered silicate, compatibilizer or surfactant, organic cation, and polymer matrix) and the preparation method, three main types of composites may be obtained when a layered silicate is associated with a polymer as shown in Scheme 1 [13].

Clay mineral/polymer composites can be prepared in several ways. However, true nanocomposites are obtained by methods that can overcome the tendency of layered silicates to form face-face aggregates. The most serious obstacle in reinforcing practicable polymers by delaminated and dispersed the silicates into their matrices is the incompatibility between the layered silicates and polymers. Therefore, the appropriate modification of external and internal surfaces of the layered silicates would generate an organophilic interaction with the hydrophobic polymers and provide the most promising ways to prepare nanocomposites, e.g. Scheme 2. According to Akelah and Moet [14], for preparing polymer/layered silicate nanocomposites, several attempts have been applied to incorporate the layered silicates with the organic polymers, depending on their physical, chemical, or mechanical interactions. The physical interaction includes method of impregnation of monomers followed by polymerization, direct adsorption of linear polymers. The chemical interaction includes grafting of polymers via coupling agents, interactions of

polymer functional groups with clays, hydrolysis of organometallics within polymeric matrices, and intercalation of polymers with organophilic clays.   Basically, Akelah and Moet emphasize synthesis method to prepare nanocomposites.   For example, the cation exchange grafting of polymers through chemical bonds to the layered silicates to produce nanophase organic-inorganic hybrids has been developed.   This technique may involve either by producing monomer-impregnating organophilic silicates first, followed by polymerized the monomers to grow the polymeric chains in the interlayers space; or by direct intercalation of positively charged polymer chains from solution to the anionic silicate layers.   Two intercalation processes, including solution polymerization and melt polymerization were adapted for producing these nanocomposites.   At present, these synthesis methods for preparing polymer nanocomposites introduced by Akelah and Moet are still adopted widely in many different polymer industries, including plastics, resins, and elastomers.

Besides synthesis or in-situ polymerization methods, now-a-days, there are many other methods to prepare the polymer nanocomposites.   Many related researches have been reported.   These methods, according their process design, are emulsion polymerization or latex blending process, solution process either by prepolymers or polymers, and melt intercalation process with internal mixers or extruders in proper formulation and process design.

Since Toyota Motor Company, a pioneered researcher of polymer nanocomposites, created Nylon 6-clay hybrid (NCH), used to make a timing-belt cover, they have had a lot of reports to focus on these fields of preparing practicable nanocomposites [15, 16].   Actually, nano-scale reinforcement should enable parts and system design of polymer composites that will be cost-competitive with other polymers, and eventually replace metals and glass, thus enabling the automotive or sporting industries to capture a leadership position in fuel-efficient, higher-quality,

and durability.

1-2 Materials

1-2-1 Nitrile rubber (NBR) and butadiene rubber (BR)

Nitrile rubber, an elastomeric copolymer of butadiene and acrylonitrile, is synthesized generally by emulsion polymerization and forms either in case a latex or a dry rubber.   The important properties trends of the copolymer are influenced by acrylonitrile content, a polar component that resulting in a high polar NBR elastomer. Nitrile rubber is available in several grades of oil resistance based on the acrylonitrile content of the elastomer raging from about 53 to 18%.   On the contrary, polybutadiene rubber, a nonpolar elastomer, can be prepared by either emulsion or solution polymerization.   Most is produced by solution polymerization in which a variety of controlled structure BR, e.g. a configuration of cis, trans, and vinyl components, etc., can be made.   Both rubbers are widely used in machinery, automobiles, and sporting industries today.

Elastomers are entropic systems characterized by a network structure (through a path of vulcanization process) which includes flexible segments of molecular chain (acting as springs), connected by chemical or physical crosslinks(acting as knots).   The flexible segments are commonly in the disordered random coil conformation in the unstretched state and assume extended conformation upon stretching.   The presence of network knots prevents the material from flowing during applying tensile or shear force.   Hence, to prepare an elastomer nanocomposite, the melt intercalation process should be properly controlled to obtain a homogeneous and well dispersed phase of layered silicate-rubber molecular chain before mature vulcanization or simultaneously.

1-2-2 Layered silicates

1-2-2.1 Structure and type

The layered silicates (usually referred to as clay minerals) are composed of stacks of hydrated alumino-silicate, in particular montmorillonite (MMT). Their crystal structure consists of two dimensional layers with thickness about 1 nm and lateral width 200-300 nm that is made up of two silica tetrahedral sheets with an edged-shared octahedral sheet of either alumina or magnesia as shown in Figure 1 [14]. Stacking of these layers results in intergalleries or interlayers due to strong van der Waals force. The interlayers of MMT are separated by sheets of hydrated inorganic cations, typically Na^+ or Ca^+, which balance the oxide layers charge and are readily ion exchanged with a wide variety of positively charged species. MMT is basically composed of aggregates having 0.1 to 10 μm particle size range that is associated by many primary particles, which, in turn, are consisted of lots of superimposed lamellae, as shown in Figure 2. Each primary particular contains approximately 8 lamellae or 16 planes. Among all the layered silicates, Na^+-MMT having the optimum cation exchange capacity (CEC), 90-120 meq/100 g, is the most frequently used nano-filler.

Variation in the amount, type, and crystallographic origin of the excess layer charge results in a large family of natural (e. g., MMT. hectorite, saponite beidellite) and synthetic (e. g., laponite, fluorohectorite) layered silicates exhibiting different characteristics, like layer size, stacking perfection, reactivity, and Lewis acidity. Two types of the major inorganic layered silicates include smectites and layered silicic acids, and the typical chemical formulas of some layered silicates are shown in Table 1.

2-2-2 Hydrated swelling and functionality modified

The physical and mechanical properties of polymer nanocomposites are significantly improved when the grains of layered silicates are reduced in size from

100 μm to several nanometer range.   These nanocomposites are multilayered sandwich-like materials in which polymer chains are intercalated between ultrathin sheets of layered silicates.   However, due to its hydrophilic nature, layered silicate is generally swelled in water to expand its intergallery space to be blended with the aqueous polymer or modified by alkylammonium surfactants to achieve enough hydrophobicity and expanding gallery to be well miscible with the organophilic polymer matrix.

Hydrated swelling   The driving force for the swelling of MMT is caused by hydration of the interlayer inorganic cations.   Water can associate with the cations to form hydration shells and complete the filling of the interlayer space.   The interlayers expansion and water packing density are affected by the density and type of cations, layer charge and its distribution, and the strength of the liquid structure rather than by the MMT silicate surface.   Water molecules having strong salvation forces and low self-preservation tendency would distribute well around the cations. In presence of larger amounts of water, the MMT becomes fully expanded and dispersed with the spacings exceed 2 nm, where fewer regular gallery can be measured by the X-ray pattern.   It also means that single silicate layer can be obtained in indefinite swelling of MMT in water and the interlayer cations no longer reside at the silicate surface.   Hence, exfoliating MMT layers dispersing well in water-soluble polymer or aqueous polymer latex would be expected.

Functionality modified   Due to most of the polymers, including plastics, elastomers, and resins are hydrophobic and water-insouble, the hydrophilic inorganic layered silicates need to be modified with the functional organomodifier to become miscibly with the polymers.   To enhance the compatibility of layered silicates with organophilic polymers, the interlayer cations are generally replaced with organic

cations (e.g., quarternary ammonium ion), called intercalation, functionalizing the

inter and outer surface of aluminosilicate.   Some type of quarternary ammonium

used to modify Na^+-MMT or other layered silicates are by replacing the sodium ion

with the following organic species [17]:

(1) n-alkylammonium ions   n=1-18

$$C_nH_{2n+1}\text{-}NH_3^+$$
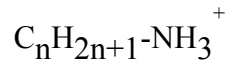
(2) N-n-alkylpyridinium ions   n=1-18

$$C_nH_{2n+1}\text{-}\overset{+}{N}\bigcirc$$
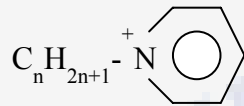
(3) N   N   N-trimethyl-N-n-alkyl-ammonium ions   n=12, 14, 16, 18

$$C_nH_{2n+1}\text{-}\overset{+}{N}\text{-}(CH_3)_3$$
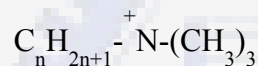
(4) N   N-dimethyl-N   N-di-n-alkyl-ammonium ions   n=8, 10, 12, 14, 16, 18

$$(C_nH_{2n+1})_2\text{-}\overset{+}{N}\text{-}(CH_3)_2$$
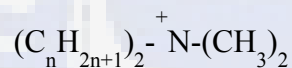
Example of cation exchange reaction is as the follow:

$$Na_2Si_{14}O_{29}\quad 11H_2O + x\,\overset{+}{M} \rightarrow M_x Na_{2-x} Si_{14} O_{29}\quad z\,H_2O + x\,\overset{+}{Na} +\quad 11\text{-}z\quad H_2O$$
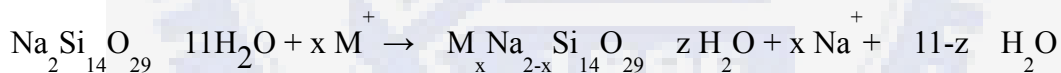
x : the fraction of sodium interlayer cations replaced

$\overset{+}{M}$: (1) and (2) are nearly quantitative ion exchange

(3) are markedly reduced for long chain

Actually, at present, several routes have been used to intercalate layered silicate

particles, including intercalation by solvents and solutions, intercalation by organic

cations, intercalation by organic liquids, by inorganic intercalants, and by melt

intercalation method.   During intercalation the intercalant molecules diffuse to the

galleries between individual silicate layers, and the basal spacings are expanded.

The process depends on the balance of forces, the size and geometry of gallery, the type, size, and structure of intercalant molecules, the matrix viscosity, etc. Depending on the charge density of the clay, the intercalant onium ions may lie parallel to the clay surface as a monolayer, a lateral bilayer, a pseudo-trimolecular layer, or an inclined paraffin structure as illustrated in Figure 3 (a) [18].   In general the basal spacing increases most nearly linearly with the chain length of the cation.   According to Lagaly et al [17], the high basal spacings of alkylammonium-magadiite have been interpreted by the following model: the alkylammonium ions are arranged in bilayers between the silicate layers, their chain axes orienting perpendicular to the silicate sheets as shown in Figure 3 (b).

1-2-3 elastomer nanocomposites

For several years, many researchers have done a lot of efforts, attempted to develop elastomer/layered silicate nanocomposites, and expected to obtain high performance nanocomposites that having superior mechanical and physical properties. However, much of such devotion has failed to produce true elastomer nanocomposites with layered silicates to replace the traditional carbon black.   There are the reasons that to achieve a true layered silicate exfoliation is difficult and there is only a week interaction force occurred between both phases of silicate and rubber matrix. Actually, most of the rubber chains are partially intercalated into the silicate galleries as the scheme 1 (b) shown, and a few are exfoliated as the scheme 1 (c) shown, which could be due to the following reasons:

The viscosity of the rubber is too high due to its higher molecular weight, that restricts the movement of the molecular chains and prevents them from moving into the silicate galleries.

The vulcanization reaction is too fast and restricts the movement of the rubber chains into the silicate galleries because of the formation of network. Thus, the

intercalation only occurs at the entrance of the galleries.

The shear force is insufficient during blending progress, and cause the 'partial' intercalation, which could be due to too higher temperature, poor process design or improper equipment.

There is little chemical reaction happened between the surface of silicate and elastomer molecular chains, which may result from non-enough compatibility of both phases.

During last decade, elastomer/layered silicate nanocomposites have been prepared by many different process methods, including emulsion polymerization or latex blending, melt intercalation, and solution process [19-24].   In this thesis, some new strategy based on the similar process was developed to prepare disorderly exfoliated nanocomposites, in which proper selection of layered silicates and rubbers are considered carefully.   Concerning the compatibility, there also have some factors to be considered, e.g. polar effect, coupling agent or surfactant with reactive functional group, compatibilizer selection, and so forth.

1-3   Research Motivation and Purpose

The interaction between inorganic or organo-modified layered silicates and the elastomer chains to enhance the physical and mechanical properties of the elastomer nanocomposites is interesting.   It needs to modify inorganic silicates to change its surface state for improving the compatibility of layered silicates with the hydrophobic elastomer.   Different processes can be designed to create a true elastomer nanocomposite, depending on polymer type and phase state, proper formulation design (material selection), proper selection of surfactant or compatibilizer, equipments used, and thermodynamics available.   When a elastomer nanocomposite is prepared, besides of the mechanical, thermal, and

barrier properties are tested, the morphology and thermodynamic properties of the nanocomposite sample would also be interested to be performed.   A true elastomer nanocomposite can exhibit superior mechanical, thermal, and processing properties and is expected to be applied suitably for sporting goods, surgical hoses or gloves, and replace metals in automotive and other application [15].   Currently, the global expectations for fuel economy and low emission for manufacturing and transportation are requested seriously and immediately.   A demand for new low-cost, high-performance, and light-weight functions would be needed, and this could also be predicted to create a series of novel polymer nanocomposites in the near future.

Reference

[1] J. E. Mark, *Polym. Eng. Sci.*, **36**, 2905 (1996).

[2] L. Matejka, K. Dusek, J. Plestil, J. Kriz, and F. Lednicky, *Polymer*, **40**, 171 (1998).

[3] Z. Ahmad, M. I. Sarwar, and J. E. Mark, *J. Mater. Chem.*, **7**, 259 (1997).

[4] T. von Werne, T. E. Patten, *J. Am. Chem. Soc.*, 121, 7409 (1999).

[5] B. Finnigan, D. Martin, P. Halley, R. Truss, and K. Campbell, *J. Appl. Polym. Sci.*, **97**, 300 (2005).

[6] M. W. Weimer, H. Chen, E. P. Giannelis, and D. Y. Sogah, *J. Am. Chem. Soc.*, **121**, 1615 (1999).

[7] A. Usuki, A. Tukigase, and M. Kato, *Polymer,* **43**, 2185 (2002).

[8] M. Maiti, S. Sadhu, and A. K. Bhowmick, *J. Polym. Sci. Part B: Polym. Phys.*, **42**, 4489 (2004).

[9] A. Ranade, N. D'Souza, C. Thellen, and J. A. Ratto, *Polym. Int.*, **54**, 875 (2005).

[10] H. A. Stratz, D. R. Paul, and P. E. Cassidy, *Polymer*, **46**, 3818 (2005).

[11] M. Krook, G. Morgan, and M. S. Hedenqvist, *Polym. Eng. Sci.,* **45**, 135 (2005).

[12] G. Kickelbick, *Prog. Polym. Sci.*, **28**, 83 (2003).

[13] M. Alexandre and P. Dubois, *Mater. Sci. Engng.*, **28**, 1 (2000).

[14] A. Akelah and A. Moet, *J. Appl. Polym. Sci.: Appl. Polym. Sympo.*, **55**, 153 (1994)].

[15] J. M. Garcés, D. J. Moll, J. Bicerano, R. Fibiger, and D. G. McLeod, *Adv. Mater.*, **12**,1835 (2000).

[16] T. W. Lee, O. O. Park, J. Yoon, and J. J. Kim, *Adv. Mater.*, **13**, 211 (2001).

[17] G. Lagaly, K. Beneke, and A. Weiss, *Am. Mineral.* **60**, 642 (1975).

[18] G. Lagaly, *Solid State Ionics,* **22**, 43 (1986).

[19] M. Song, C. W. Wong, J. Jin, A. Ansarifar, Z. Y. Zhang, and M. Richardson, *Polym. Int.*, **54**, 560 (2005).

[20] K. G. Gatos, N. S. Sawanis, A. A. Apostolov, R. Thomann, and J. Karger-Kocsis, *Macromol. Mater. Eng.*, **189**, 1079 (2004).

[21] W. F. Dong, Y. Q. Liu, X. H. Zhang, J. M. Gao, F. Hwang, Z. H. Song, B. H. Tan, and J. L. Qiao, *Macromolecule*, **38**, 4551 (2005).

[22] Z. F. Wang, B. Wang, N. Qi, H. F. Zhang, and L. Q. Zhang, *Polymer*, **46**, 719 (2005).

[23] Z. J. Zhang, L. Zhang, Y. Li, and H. D. Xu, *Polymer,* **46**, 129 (2005).

[24] M. Y. Liao, W. Shan, J. D. Zhu, Y. Li, and H. D. Xu, *J. Polym. Sci : Part B: Polym. Phys.*, **43**, 1344 (2005).

Scheme 1. Different types of composites arising from the interaction of layered silicates and polymers: (a) phase-separated microcomposite; (b) intercalated nanocomposite and (c) exfoliated nanocomposite. [Referring to : M. Alexandre and P. Dubois, *Mater. Sci. Eng.*, **28**, 1 (2000)]

Layered silicate   Polymer

(a)
Phase separated
(microcomposite)

(b)
Intercalated
(nanocomposite)

(c)
Exfoliated
(nanocomposite)
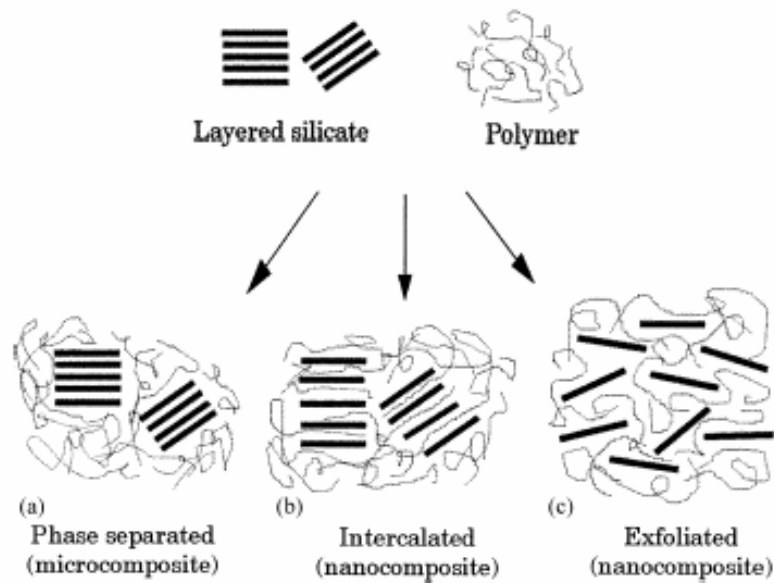
Scheme 2. Surface modification via compatibilizer

Particulate   Compatibilizer   Matrix   Composite
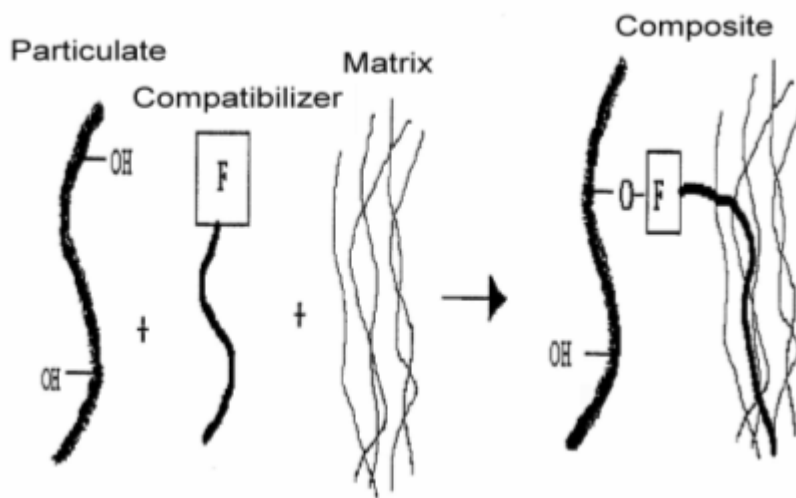
Table 1 : Characteristic properties of layered silicates

(a) Typical example of structure and chemistry of smectites commonly used.

	Montmorillonite	Hectorite	Saponite	Fluorohectorite	Laponite
Type	Dioctahedral	Trioctahedral	Trioctahedral	Trioctahedral	Trioctahedral
Substitution	Octahedral	Octahedral	Tetrahedral	Octahedral	Octahedral
Unit Cell	$M_x[Al_{4-x}Mg_x]$	$M_x[Mg_{6-x}Li_x]$	$M_{y-x}[Mg_{6-x}Fe_x^{3+}]$	$Li_{1.12}[Mg_{4.88}]$ $Li_{1.12}$	$Na_{0.7}[Mg_{5.4}]$ $Li_{0.4}$
Formula (X~0.67)	$Si_8O_{20}(OH)_4$	$Si_8O_{20}(OH)_4$	$Si_{8-y}Al_yO_{20}(OH)_4$	$[Si_8O_{20}]F_4$	$Si_8O_{20}(OH)_4$

M: exchangeable cation, like Na^+.

(b) Examples of layered silicic acids.

Layered silicic acids	Chemical composition	Interlayer spacing, d_{001}, nm
Kanemite	$NaHSi_2O_5$ $7H_2O$	~1.03
Makatite	$Na_2Si_4O_9$ $5H_2O$	~0.903
Octosilicate	$Na_2Si_8O_{17}$ $9H_2O$	~1.10
Magadiite	$Na_2Si_{14}O_{29}$ $11H_2O$	~1.56
Kenyaite	$Na_2Si_{20}O_{41}$ $10H_2O$	~1.20
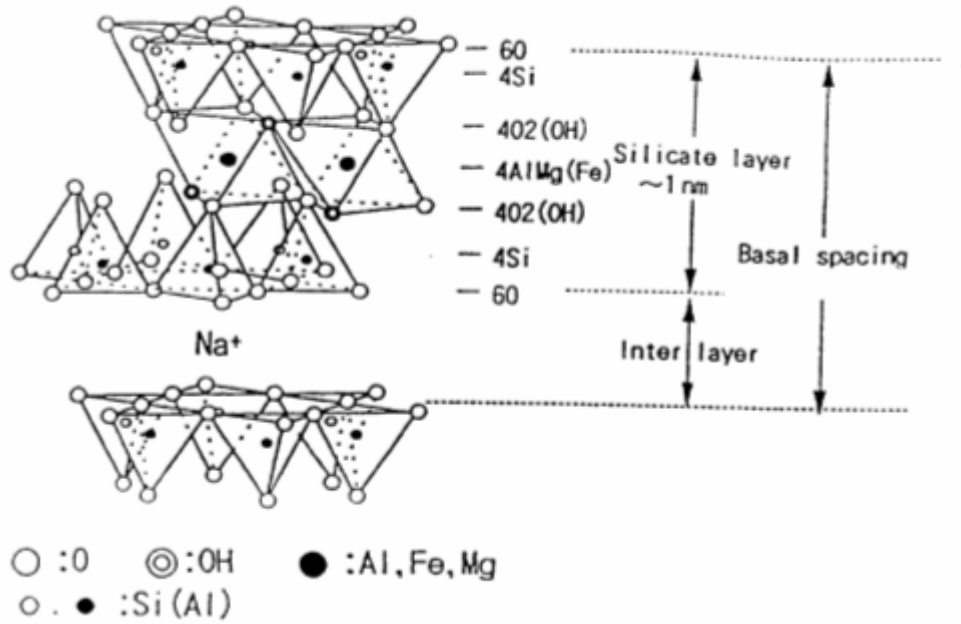
Figure 1. Structure of montmorillonite (Na^+-MMT). [reproduced according to A. Akelah and A. Moet, *J. Appl. Polym. Sci.: Appl. Polym. Sympo.*, **55**, 153 (1994)]
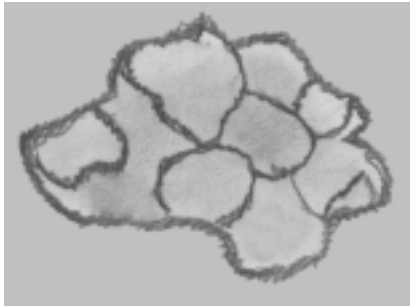
Agglomerate consisting of microaggregate

Microaggregate consisting of primary particles

Simply intercalate tactoids (primary particles)

How to obtain exfoliated layered silicates ?

Figure 2. Layered silicate (Na^+-MMT) basically composed of aggregates that is associated by many primary particles, which, in turn, are consisted of lots of superimposed lamellae.

(a) Orientations of alkylammonium ions in the galleries of layered silicates with different layer charge densities [Lagaly, 1986].
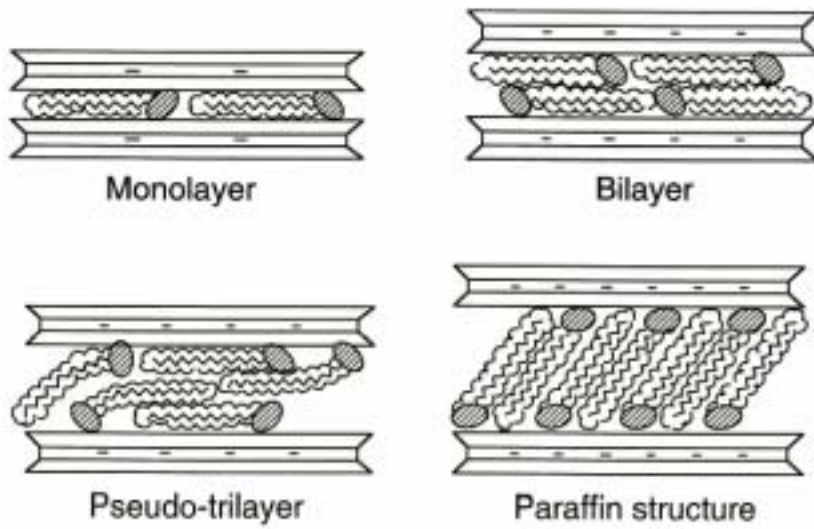
(b) The alkylammonium ions arranged in bilayers between the silicate layers, their chain axes orienting perpendicular to the silicate sheets [reproduced according to Lagaly et al, 1975].
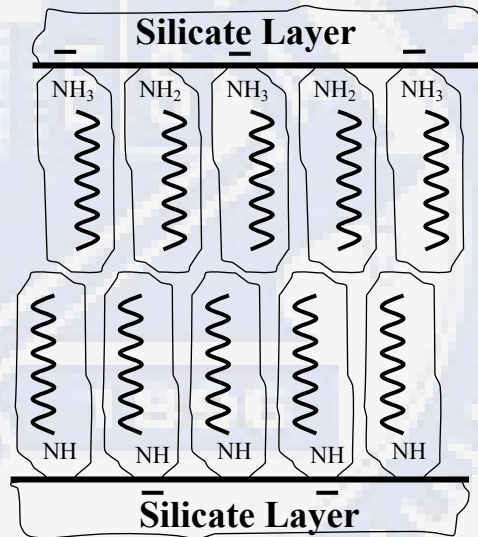
Figure 3. (a) Orientations of alkylammonium ions in the galleries of layered

silicates with different layer charge densities [18].

(b) The alkylammonium ions arranged in bilayers between the silicate

layers, their chain axes orienting perpendicular to the silicate

sheets [17].

Chapter 2: Preparation and Mechanical Properties of Nitrile Butadiene Rubber/Silicate Nanocomposites

2-1 Introduction

Layered silicates/polymer nanocomposites combine the easy processing of polymers with the strength of nanometer-sized layered silicates having one dimension about 1 nm.   These nanocomposites can exhibit synergistic properties from individual components without causing large detrimental effect to their original properties by incorporating only a small percentage of layered silicates, thus providing a new technological and economic route for the production of potentially valuable materials.   Nylon 6-silicate is the first example of those hybrid composites [1].   Other polymer-layered silicate nanocomposites, involving materials such as polyimide [2-4], polyurethane [5-7], polyolefins [8-10], polyisoprene rubber [11] and silicone elastomer [12], have also been reported recently.

Only a few cases of elastomer nanocomposites consisting of various rubbers and layered nano-silicates have ever been reported [13-15].   Different methods of intercalation of layered silicates, such as melt intercalation, in-situ polymerization and latex shear blending methods, have been adopted to prepare the elastomer nanocomposite.   Specifically, some organo-modified silicate reinforced elastomer nanocomposites, obtained from a melt intercalation method, have been reported by the high shear force generated in a plasticorder or a twin-screw extruder [15-22].   For instance, ethylene propylene diene methylene linkage rubber-clay hybrid has been prepared successfully by melt mixing of EPDM and organophilic clay in a plasticorder followed by vulcanization process [16].   On the other hand, a shear blending process on elastomer latex produces a poor intercalation and dispersion

morphology of silicate layers [23-26].

Nitrile butadiene rubber (NBR), in the solid or latex state, is one of the most widely used, commercialized and mass-productive elastomers that is manufactured mostly by the emulsion polymerization method. In the present study, NBR/silicate nanocomposites are prepared using a modified latex shear blending method. The source of layered silicate utilized in this study is Na^+-montmorillonite (MMT), which consists of a lamellar structure that is constructed from an octahedral alumina sheet sandwiched between two tetrahedral alumina sheets. The surfaces of these silicate layers contain negative charges with strong van der Waals interaction forces that are balanced by Na^+ cations absorbed on the near- surface to compensate for the net negative charge. When the inorganic layered silicates are dispersed in water, the interlayer spacing largely expand due to hydrogen bonding, which enables relatively larger-sized molecules, such as surfactants, to penetrate into their galleries [27-29]. Then, the enlarged galleries could allow even larger molecules to diffuse and intercalate into the interlayer space. NBR/silicate nanocomposites could not be easily prepared by melt intercalation as a result of the poor miscibility of NBR with layered silicates. In the present study, a new intercalation process is used to produce nanocomposites by shear blending of nitrile latex with surfactant-treated hydrophilic layered silicates, and the resulting mechanical properties of these nanocomposites are investigated.

2-2. Experimental Methods and Analysis

2-2.1 Materials

Nitrile butadiene rubber latex (NBR latex, Nancar 1052) containing 31-33% acylonitrile was obtained from Taiwan Nancar Co. Ltd., with a solid content of about 27%. Clay Swy-2 (Wyoming Na^+-montmorillonite, i.e. Na^+-MMT), having a

cationic exchange capacity (CEC) of 76.4 meq./100g, was provided from the Clay

Minerals Depository at the University of Missouri, Columbia, MO.   Aromatic

polyglycol ether (Emulvin W), a nonionic emulsifier acting as a emulsifying,

stabilizing and wetting agent for latexes, was acquired from Mobay Co. Ltd.   Other

ingredients, such as the surfactant (sodium salt of methylene- bis-naphthalene

sulphonic acid), dispersing agent and curing agent were supplied from a local agency

(R.T. Vanderbilt Co. Ltd., Taiwan).

2-2.2 Latex blending and sample preparation

The last number behind the sample notation, NX-, stands for different content of

layered silicates, which was added to NBR latex.   For example, NX-0 is neat NBR,

and NX-10 contains 10wt% layered silicates in NBR.   Typical industrial

formulations were used in this study.   A mixture of Na^+-MMT , dispersing agent,

emulsifier, potassium hydroxide (electrolyte) and deionized water was placed in a

ball-mill tank to produce a homogeneous, swelled and intercalated layered silicate

solution.   The cure agents, including 0.5 phr (parts per hundred rubber) sulfur and

proper amounts of accelerator, zinc oxide, oleic acid, dispersing agent, emulsifier, and

potassium hydroxide, were also mixed and prepared as a slurry at the same time.

Subsequently, each clay solution was individually added to the nitrile butadiene

rubber latex and blended for 48 hours to form a homogeneous latex composite.   Then,

each batch of curing slurry was added to the latex composite and blended an

additional 48 hours.   Afterward, each batch of latex composite was poured directly

into a flat plate vessel, dried for 24 hours in a 50 ^{o}C hot air oven, washed with water

and cured for 4 hours at 110 ^{o}C to obtain a rubber slab.   Each slab was controlled to

an approximate thickness of 1 mm.

In the present study, a well-dispersed layered silicate water slurry was prepared

by mechanical ball milling of an emulsified solution with an adjustment of its pH

value.   Then, it was blended with the prepared nitrile latex, using normal stirring for

a proper period of aging time.   It was found that most of the homogeneous

nanocomposite latexes were stable even after one month when stored at room

temperature.

2-2.3 Characterization

Wide-angle X-ray diffraction (XRD) measurements were carried out with a

Mac Science M18 X-ray diffractometer.   The X-ray beam was produced by

nickel-filtered Cu Kα radiation with wavelength $\lambda = 0.154$ nm operated at 30 kV and

25 mA.   The diffraction curves were obtained within the range of scattering angles

(2θ) of $2\text{-}10^{o}$ at a scan rate of $1 \ ^{o}/min$.   The TEM used is a JEOL JEM 2000FX

electron microscope operating with an acceleration voltage of 100 kV.   Ultrathin

sections of the cured samples were microtomed using Leica Ultracut Uct into about

100-nm thick slices with a diamond knife; subsequently, a layer of carbon was

deposited onto these slices and placed on 400 mesh copper nets.

Thermogravimetric analysis (TGA) of each sample was carried out under nitrogen

purge in a Perkin-Elmer TGA-7.   About 10 mg of cured sample was heated from

50 to 700 ^{o}C at 10 ^{o}C / min.   Both the tensile and tear strength of the cured rubber

slab were tested on a MTS tensile tester, Sintech 1-D, according to the ASTM

standard D412-97 method, die C and D624-95 method, die B, respectively.

2-3 Results and Discussions

The dispersion image of layered silicates on the NBR matrix are shown and

discussed individually in the section 2-3-A for the NBR-layered silicate

nanocomposites.   The mechanical properties and the mechanism scheme of the

NBR-layered silicate nanocomposites are discussed in the section 2-3-B and 2-3-C,

respectively.

2-3-A.   Layered silicates dispersion in NBR nanocomposites

Figure 2A-1 shows the X-ray diffraction curves for the cured NBR/silicate nanocomposites.   The X-ray diffraction peaks at $2\theta = 6.84^{o}$, 2.73^{o}, 2.63^{o} and 2.65^{o} represent the diffraction of the (001) crystal surface of layered silicates in the nanocomposites, corresponding to d-spacings of 1.29, 3.23, 3.36 and 3.33 nm, respectively.   This indicates that a relatively large gallery expansion in layered silicates has been obtained in the case of NX-3 , NX-5 and NX-7.5.   For the NX-5 sample, the major peak appears around 2.63^{o}, and a blurred peak appears at about 3.33^{o} (2.65nm), which might be caused by non-uniform expansion of layered silicates. For the NX-7.5 sample, other than the diffraction of X-ray by the (001) plane at about $2\theta = 2.65^{o}$, another strong diffraction peak can be observed at about 5.36^{o} (1.65nm). This probably indicates that there has a bimodal structure for layered silicates in NBR when the amount of layered silicates is over about 5 wt%.   Figure 2A-2 presents TEM micrographs of the dispersion of nanometer-sized layered silicates in the NBR film.   Single silicate layers in the rubber matrix and a few multi-layer bundles in the case of NBR containing 3 and 5 wt% layered silicates can be found in Figure 2A-2 (a) and (b).   In both cases, the exfoliated layered silicates, where the interlayer d-spacing was larger than 3.2 nm, can be observed; whereas, in Figure 2A-2 (c), the dispersion of silicates in NBR can be found to actually adopt a bimodal structure, consisting of both intercalated and exfoliated states.   This reveals that a higher silicate loading would lead to poorer dispersion and more aggregated bundles in the rubber film.   A critical concentration of 7.5 wt% layered silicate in NBR/silicate nanocomposites can be utilized to exert the exfoliated nanocomposite using the modified latex shear blending method.   The results of the TEM analysis correspond to those of the X-ray analysis quite well.   Hence, based upon the results of XRD and TEM, it is likely that

in the nanocomposites of NBR with silicate concentrations between 3 and 7.5 wt%, exfoliated and partially intercalated layered silicates coexist .

2-3-B.   Mechanical and thermal properties of NBR nanocomposites

2-3-B.1 Mechanical properties

The stress-strain curves of these crosslinked NBR/silicate nanocomposites are shown in Figure 2B-1.   At low strains, these materials behave similarly, but the tensile modulus of NX-7.5 increases dramatically at high strains, which is different from that of neat NBR (NX-0).   The low strain behavior results from somewhat low sulfur content (low crosslink density).   The addition of nano-silicate can enhance the tensile modulus of NBR.   It can also be reasonably assumed that the dramatic increase in stress of NX-7.5 in the high strain region results from the effect of molecular chain orientation and the resultant orientation of layered silicates brought about by the rubber molecular orientation.

The effects of layered silicates content on the tensile and tear mechanical properties of the crosslinked NBR/silicate nanocomposites are illustrated in Figure 2B-2 and 2B-3.   The tensile strength increases by more than 200 %, with a slight effect on the elongation, and the tear strength also increases considerably for these NBR/silicate nanocomposites, compared to neat NBR.   The tear properties of these crosslinked NBR/silicate nanocomposites display the similar trend to that of their tensile mechanical properties.   Additionally, the tensile strengths at 500% elongation (M500, engineering modulus) of the NBR/silicate nanocomposites are also much higher than that of neat NBR.   The engineering modulus is an indicator of the stiffness of the rubber compounds.   The tensile and tear strengths of the NBR/silicate nanocomposites increase with the amount of layered silicates up to 7.5 wt%, but decrease at 10 wt% concentration.   The maximum increases in the tensile

and tear strength are about 200% and 60%, respectively.   It can therefore be

concluded that tensile and tear properties of NBR can increase dramatically with a

layered silicates content up to 7.5wt% using a modified shear blending system,

where the molecular chain motion of NBR into the galleries of largely exfoliated

nano-silicate platelets prepared by a ball milling process.   Second, exfoliated

layered silicates with finer dispersion can be established with the assistance of small

molecular, non-ionic and ionic surfactants and through the use of high shear forces

in the ball milling process.

2-3-B.2 Thermal properties

Thermal degradation temperatures (at 5% weight loss) of NBR/silicate

nanocomposites also increase with the content of layered silicates.   Figure 2B-4

gives a detailed thermal gravimetric analysis of neat NBR and two nanocomposites.

In addition to improving the initial decomposition temperature, the weight loss due

to the thermal pyrolysis of NBR is nearly constant, until a temperature of about 450

^{o}C is reached.   At higher temperature, the layered silicates inhibit weight loss in

NBR.   This is possibly due to the presence of layered silicates dispersed

homogeneously in the NBR matrix that could extend the total immigration out-paths

of small molecules, as well as inner volatiles, and would reduce the permeability of

oxygen into the bulk of the nanocomposite.   Therefore, it could inhibit the

occurrence of NBR chain scission and improve the thermal stability.

2-3-C.   Schematic drawings of latex blending mechanism

Schematic drawings of the ball milling and latex blending mechanism are

provided in scheme 1 and 2, respectively.   In scheme 1, the intergallery space of

layered silicates in water is largely expanded since the appearance of the silicate

solution is homogeneous and transparent.   Then, the ball milling process generates

a proper shear force to delaminate the layered silicate and allow the surfactant molecules to move into the interspace of layered silicate. In scheme 2, after mixing with the rubber latex, the emulsified and well-expanded layered silicates can allow the elastomer molecular chains to diffuse and intercalate into the silicate galleries. After coagulating, nearly exfoliated and partly intercalated elastomer nanocomposite can form.

2-4　Conclusions

NBR/silicate nanocomposites, with a mostly exfoliated and partially intercalated coexisting structure, were successfully prepared by ball milling of surfactant-treated layered silicates in emulsified solution, followed by latex shear blending. The tensile mechanical properties and tear strengths of these nanocomposites increase with the amount of layered silicates, as compared to that of neat NBR. Additionally, these nanocomposites display higher thermal stabilities than neat rubber.

References

[1] A. Usuki, M. Kawasum, Y. Kojima, Y. Fukushima, A. Okada, T. Kurauchi, and O. Kamigaito, *J. Mater. Res.,* **8**, 1179 (1993).

[2] H. L. Tyan, Y. C. Liu, and K. H. Wei, *Chem. Mater.,* **11**, 1942 (1999).

[3] T. Agag, T. Koga, and T. Takeichi, *Polymer,* **42**, 3399 (2001).

[4] L.Y. Jiang, C. M. Leu, and K. H. Wei, *Adv. Mater.,* **14**, 426 (2002).

[5] T. K. Chen, Y. I. Tien, and K. H. Wei, *Polymer,* **41**, 1345 (2000).

[6] Y. I. Tien and K. H. Wei, *Macromolecules,* **34**, 9045 (2001).

[7] J. Ma, S. Zhang, and Z. Qi, *J. Appl. Polym. Sci.,* **82**, 1444 (2001).

[8] M. Kawasumi, N. Hasegawa, M. Kato, A. Usuki, and A. Okada, *Macromolecules,* **30**, 6333 (1997).

[9] E. Passaglia, W. Bertuccelli, and F. Ciardelli, *Macromol. Symp.,* **176**, 299 (2001).

[10] E. A. Manias, L. Touny, K. E. Wu, B. L. Strawhecker, and T. C. Chung, *Chem. Mater.,* **13**, 3516 (2001).

[11] Y. T. Vu, J. E. Mark, L. H. Phom, and M. Engelhardt, *J. Appl. Polym. Sci.,* **82**, 1391 (2001).

[12] K. S. Kwan, D. A. Harrington, P. A. Moore, J.R. Hahn, J. V. Degroot, and G. T. Burns, *Rubber Chem. Technol.,* **71**, 630 (2001).

[13] J. T. Kim, T. S. Oh, and D. H. Lee, *Polym. Int.,* **52(7)**, 1058 (2003).

[14] J. T. Kim, T. S. Oh, and D. H. Lee, *Polym. Int.,* **52(7)**, 1203 (2003).

[15] S. Varghese and J. Karger-Kocsis, *J. Appl. Polym. Sci.,* **91(2)**, 813 (2004).

[16] A. Usuki, A. Tukiguse, and M. Kato, *Polymer*, **43**, 2185 (2002).

[17] C. Nah, H. J. Ryu, S. H. Han, J. M. Rhee, and M. H. Lee, *Polym. Int.,* **50**, 1265 (2001).

[18] Y. W. Chang, Y. Yang, S. Ryu, and C. Nah, *Polym. Int.,* **51**, 319 (2002).

[19] S. Joly, G. Garnaud, R. Ollitrault, and L. Bokobza, *Chem. Mater.,* **14**, 4202 (2002).

[20] Z. Wang and T. Pinnavaia, *Chem. Mater*., **10** 3769- (1998).

[21] T. K. Chen, Y. I. Tien, and K. H. Wei, *J. Polym. Sci.: Chem*., **37**, 2225 (1999).

[22] A. Akelah and A. Moet, *J. Appl. Polym. Sci*., **55**, 153 (1994).

[23] Y. Wang, L. Zhang, C. Tang, and D. J. Yu, *Appl. Polym. Sci.*, **78**, 1879 (2000).

[24] M. Xiong, L. Wu, S. Zhou, and B. You, *Polym. Int.* **51**, 693 (2002).

[25] L. Zhang, Y. Wang, Y. Sui, and D. *Yu, J. Appl. Polym. Sci.*, **78**, 1873 (2000).

[26] Y. P. Wu, L. Q. Zhang, Y. Q. Wang, Y. Liang, and D. S. Yu, *J Appl. Polym. Sci.*, **82**, 2842 (2001).

[27] K. E. Strawhecker and E. Manias, *Chem. Mater.,* **12**, 2943(2000).

[28] T. Yui, H. Yoshida, H. Tachibana, D. A. Tryk, and H. Inoue, *Langmuir*, **18**, 891 (2002).

[29] Y. K. Kim, Y. S. Choi, K. H. Wang, and I. J. *Chung, Chem. Mater.*, **14**, 4990 (2002).
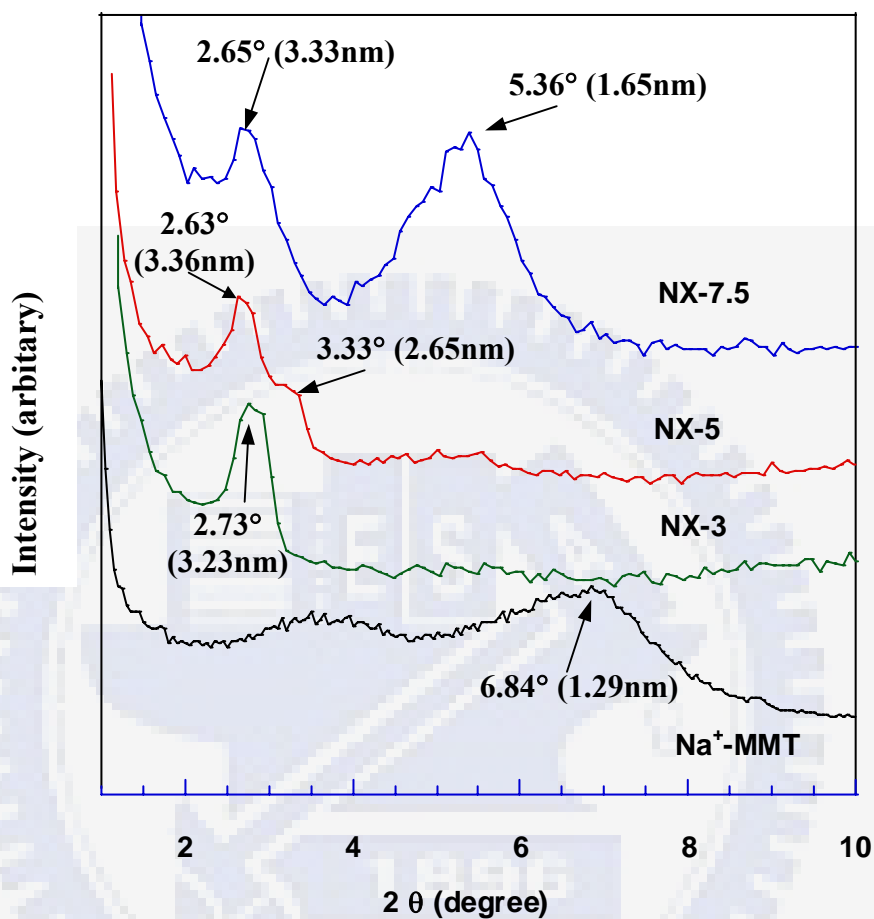
Figure 2A-1. X-ray diffraction patterns for layered silicate (Na^{+}-MMT)

and for NBR/silicate nanocomposites.
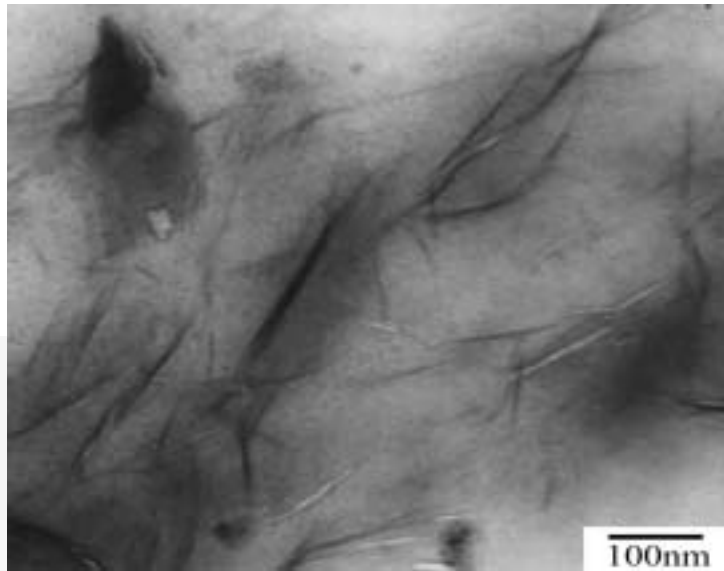
Figure 2A-2. TEM micrographs of NBR/silicate nanocomposites containing

3 wt% layered silicates. (a) NX-3 (layered silicates : 3 phr)
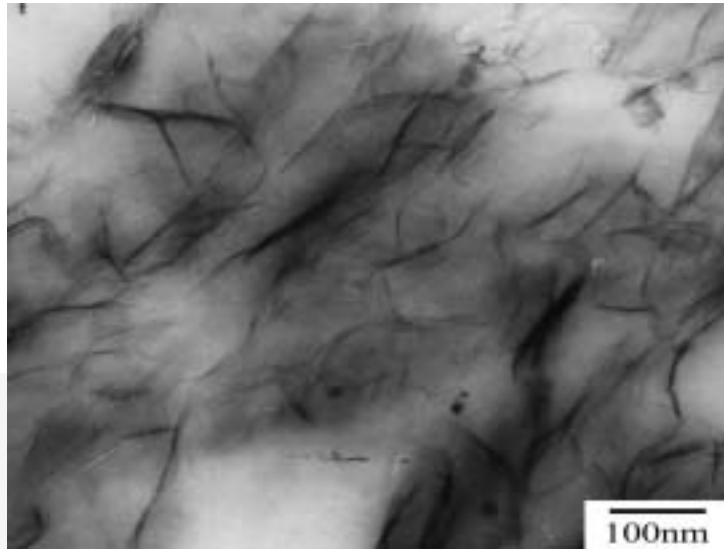
Figure 2A-2. TEM micrographs of NBR/silicate nanocomposites containing

5 wt% layered silicates. (b) NX-5 (layered silicates : 5 phr)
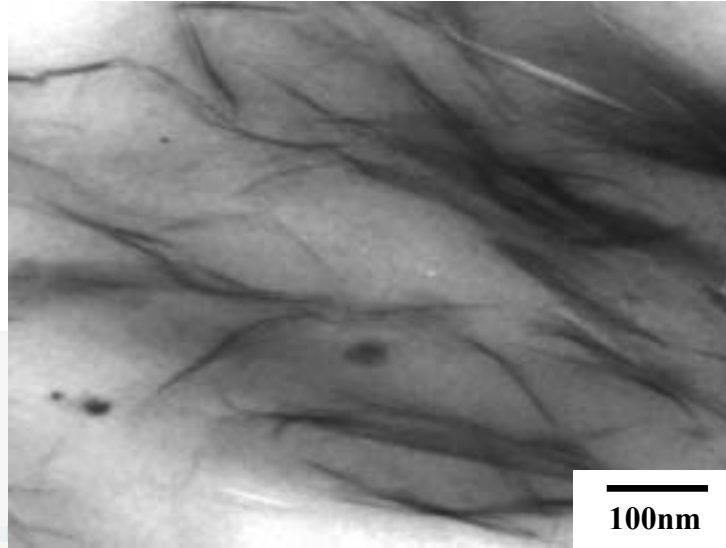
Figure 2A-2. TEM micrographs of NBR/silicate nanocomposites containing

7.5 wt% layered silicates. (c) NX-7.5 (layered silicates : 7.5

phr)
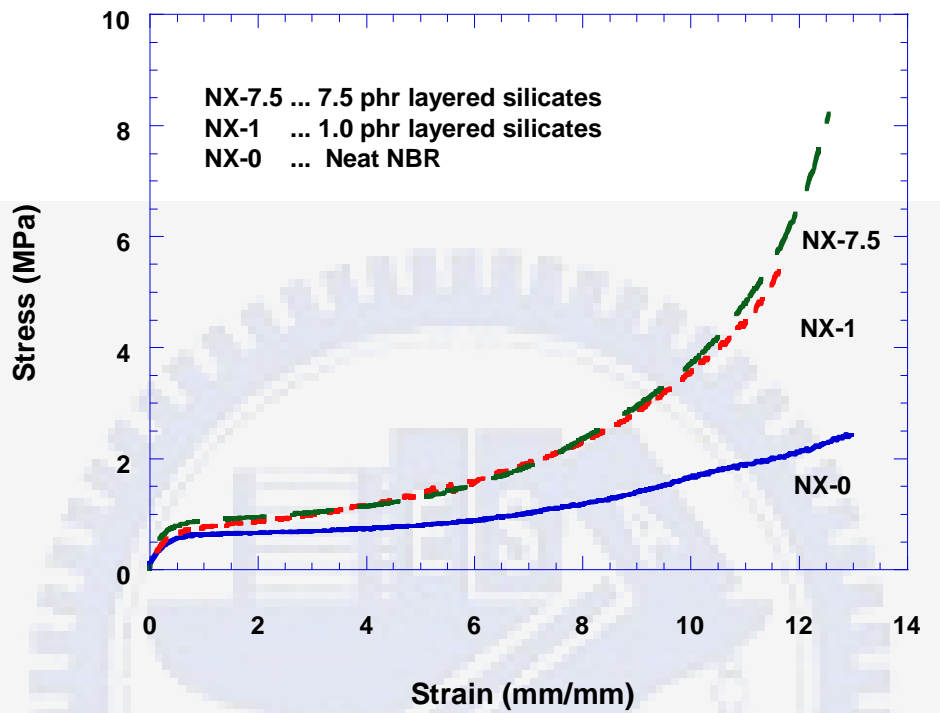
Figure 2B-1. Typical stress-strain behavior of various NBR/silicate

nanocomposites.
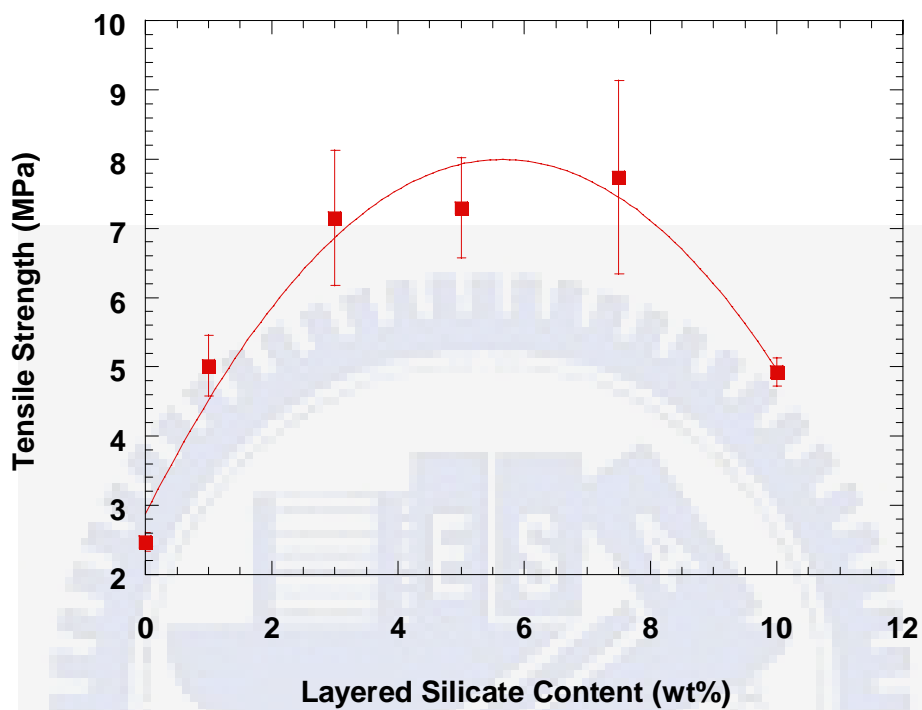
Figure 2B-2. Curves of tensile properties versus layered silicate content (wt%) of

NBR/silicate nanocomposites.   a. Tensile strength.
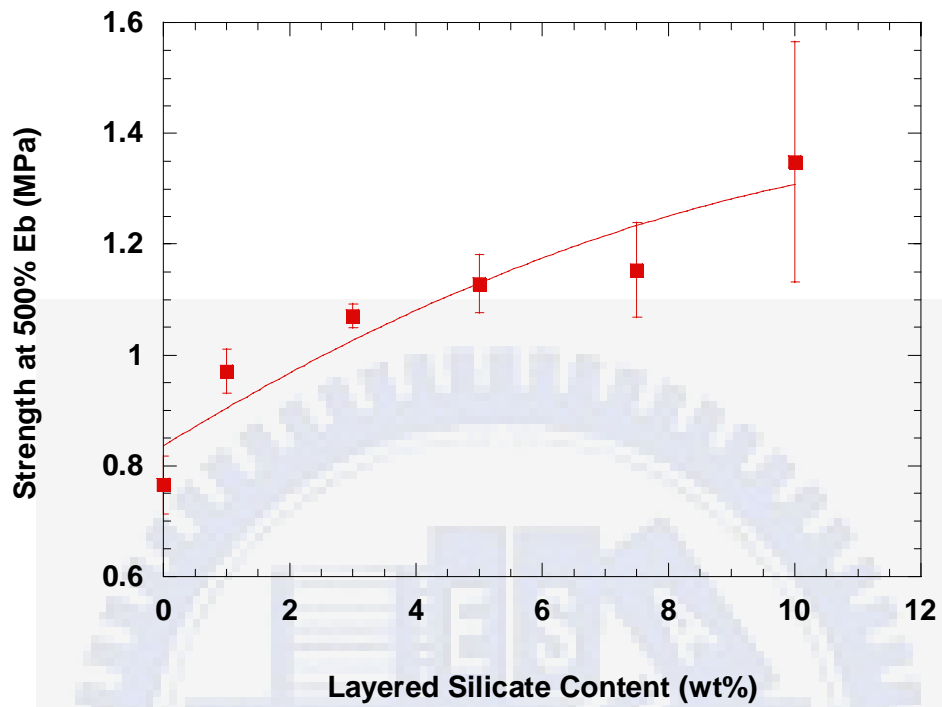
Figure 2B-2. Curve of tensile properties versus layered silicate content (wt%) of

NBR/silicate nanocomposites.   b. M500 (Engineering modulus).
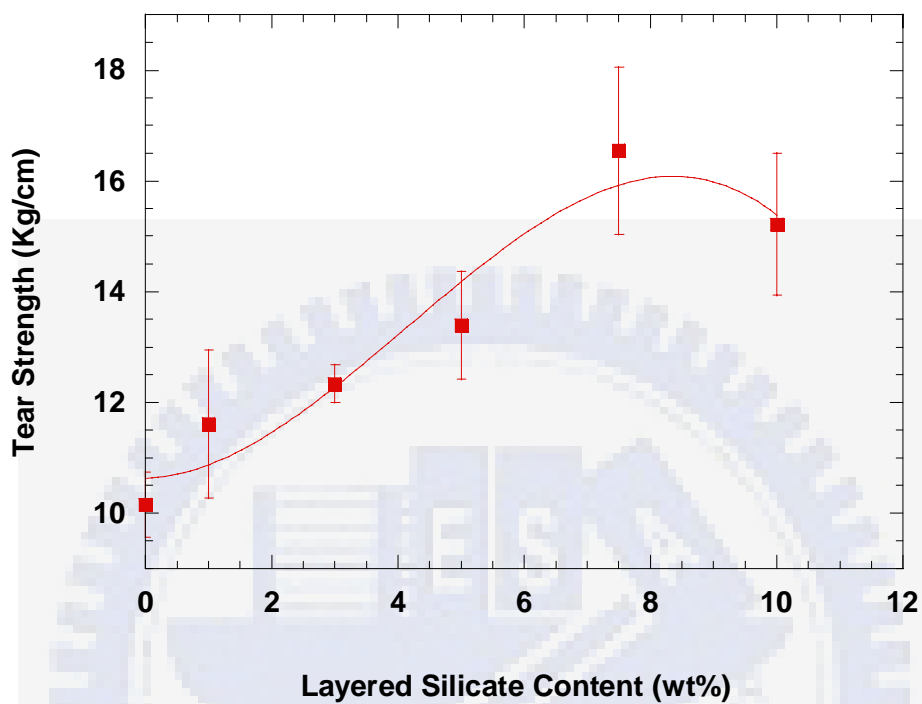
Figure 2B-3. Curve of tear strength versus layered silicate content (wt%) of

NBR/silicate nanocomposites.
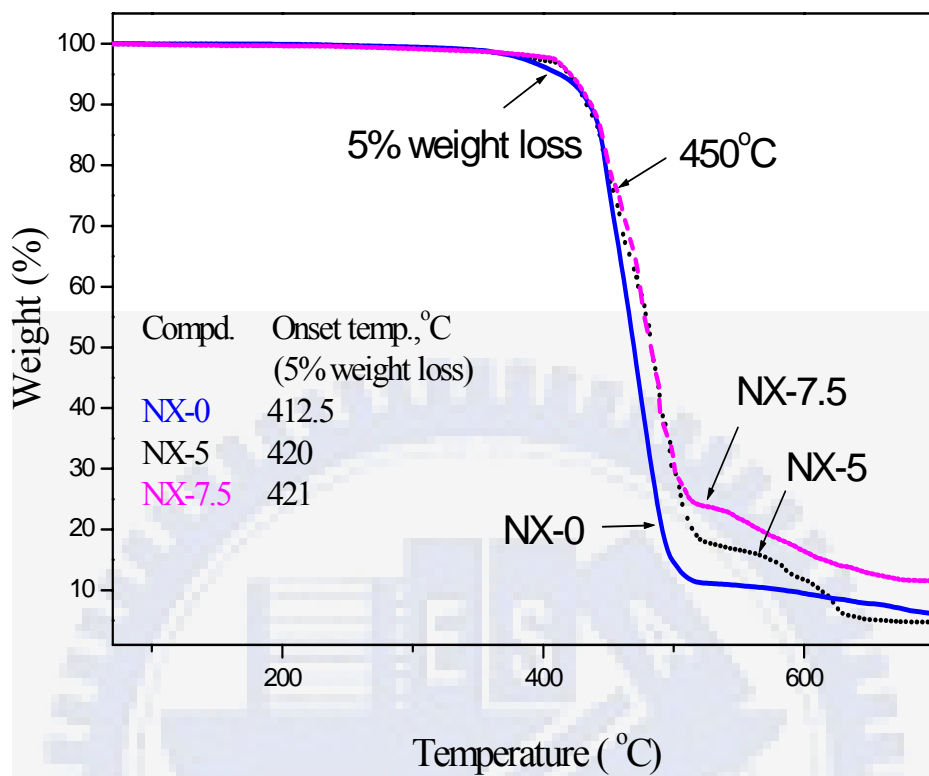
Figure 2B-4. Comparative TGA results (5 % weight loss decomposition

temperature, Td, ^{o}C) of NBR/silicate nanocomposites with neat

NBR.

2-19

Scheme 1. Formation of exfoliated layered silicates
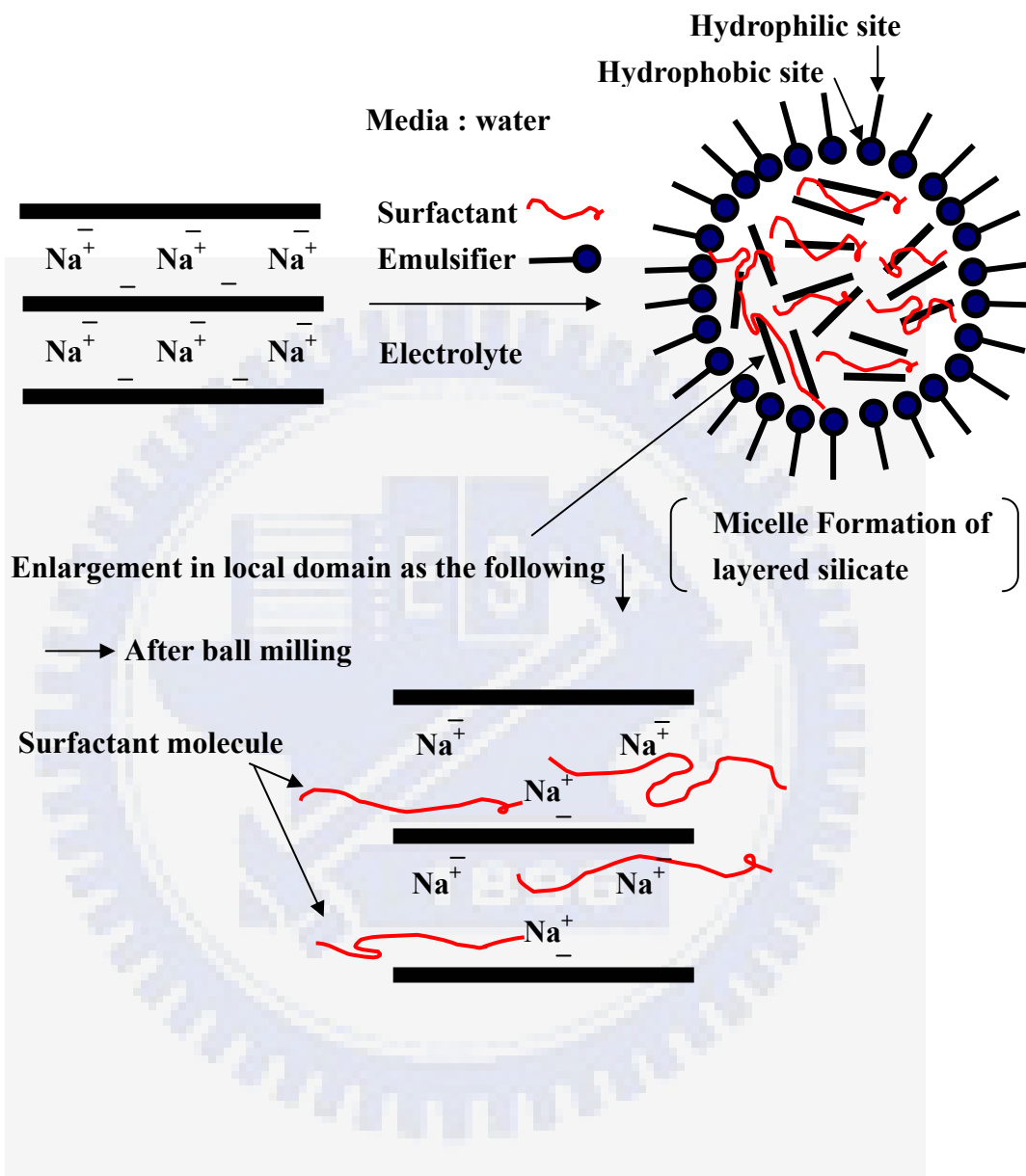
Scheme 2. Latex blending process
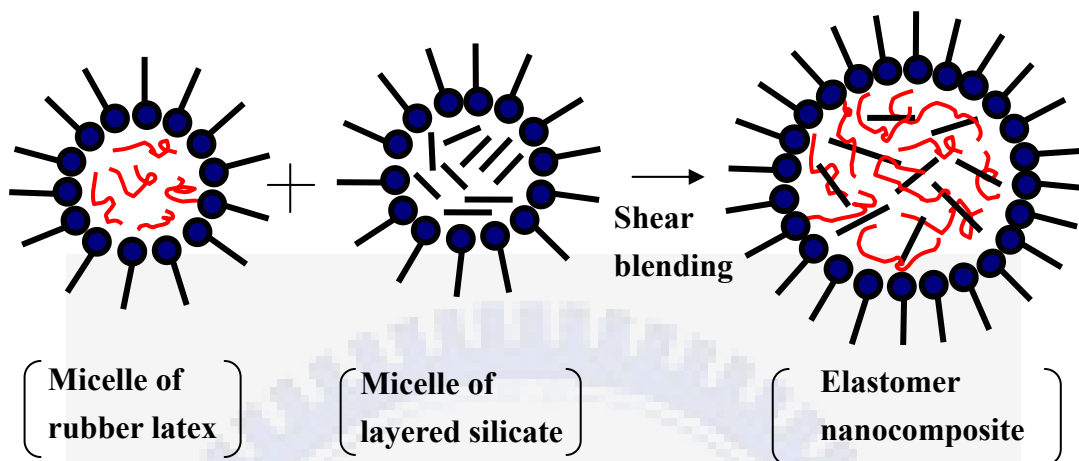
| Micelle of rubber latex | Micelle of layered silicate | Elastomer nanocomposite |

Chapter 3: Mechanical, Thermal, and Barrier Properties of NBR/Organosilicate Nanocomposites

3-1 Introduction

The pioneering work conducted by Toyota Central Research on nylon-6/silicate nanocomposites has inspired great interest in polymer nanocomposites over the past decade [1-3].   This particular interest results from the highly efficient enhancement of the barrier and mechanical properties of a polymer by the nanometer-sized silicates when they are well-dispersed in the polymer matrix.   The ideal case would have the layered silicates completely separated from one another (termed delaminated or exfoliated) in the polymer matrix.   In the other case, there would be a slight increase in the intergallery spacing of the layered silicates but the same orientation for most of layered silicates (termed intercalated) is retained in the matrix.   Exfoliation, however, can hardly be achieved in silicates without modification by small organic molecules, which diffuse readily into the intergallery of the silicate layers and open up with enough space between silicates to allow further penetration of the polymer molecules. The driving force for exfoliation or intercalation depends upon the thermodynamic interaction between polymer and silicate as well as the diffusion of polymer chains into the intergallery of the silicate layers.   In most cases, proper chemical treatment and optimized processing are key to the formation of nanocomposites. The interlayer distance of the montmorillonite-based silicates when modified with alkylammonium cations is between 1.5 and 3.5 nm.   This space is usually large enough to produce intercalated and exfoliated structures upon further processing.   In-situ polymerization, polymer intercalation from solution, and direct polymer melt

intercalation have been developed to prepare polymer-layered silicate nanocomposites [4, 5].

While organosilicates have been used in various thermoplastics and thermoset resins, a fairly small number of studies have been reported on the use of organosilicates to reinforce rubber. "Bound rubber", a traditional concept, can be used to demonstrate the reinforcing behavior of rubber with carbon black or layered silicates, which is an undissolved composition of rubber compound by solvent [6-8]. Bound rubber based on carbon black would cause a considerable increase in compounding viscosity and is disadvantageous in the mixing process. Another drawback of carbon black is that it has a black color and is usually used in high amounts, which is detrimental to the final performance of rubber formulations. A variety of white or pale fillers have been chosen to replace carbon black, such as silica or clay minerals. The reinforcing effect of NBR nanocomposites containing a few weight percent of layered silicates is similar to NBR compounds having a much higher loading of carbon black. When using properly treated organosilicate, however, it can provide an effective physical reinforcement, helping to reduce the viscosity of the uncured elastomeric compound and also retain transparency [8-10]. Additionally, the efficiency of the silicates in modifying the properties of the rubber is largely determined by the degree of their dispersion and the extent of exfoliation in the rubber. Rubbers are more hydrophobic than some of thermoplastics, such as nylon 6, and therefore, it is difficult to achieve dispersion of layered silicates in a rubber matrix by treating montmorillonite with alkyl ammonium ions alone. There are, however, some advantages for rubber/silicate nanocomposites. First, amine-compounds are widely used in sulfur curing rubber formulations as accelerators, and hence the ammonium molecule in the montmorillonite might be involved in the sulfur curing reaction. Besides, the very high molecular weight

rubber material implies that high shear stress will be generated locally during compounding, which is beneficial to the delamination of layered silicates. Hence, compounding with the proper rubber formulation design allows the intercalation and delamination of silicate layers in rubber to become possible [11]. From the literature, the use of organosilicates as precursors for the nanocomposite formations has been extended into various elastomer systems including natural rubber (NR) [12-14], epoxidized natural rubber (ENR) [6, 15], styrene butadiene rubber (SBR) [9, 16], ethylene-propylene-diene rubber (EPDM) [2, 17], nitrile butadiene rubber (NBR) [18-20], polyurethane elastomer [10, 21-23] and silicone rubber [24, 25]. The compounding methods used in these cases can be divided into solution blending, melt mixing and latex compounding. It has been shown that solution blending is a reproducible method to intercalate the rubber molecules into the silicate galleries. Solution blending of the polar NBR rubber and layered silicates has not yet been reported.

In order to a get more detailed expression on the reinforcing effect of organosilicate in rubbers, NBR was selected to produce nanocomposites by solution blending with hydrophobic organosilicates. NBR, having high polarity and being one of the most important industrial raw materials, is worthy to be surveyed. The effect of the amount of organosilicate on the mechanical, thermal and barrier properties of these nanocomposites was investigated in the present study. In addition, the thermodynamical behavior of NBR/layered silicate nanocomposites was also studied.

3-2 Experimental Methods and Analysis

3-2.1 Material preparation

Acrylonitrile-butadiene rubber (NBR, Nipol N32, acrylonitrile content 32%,

Zeon Inc., Japan) was selected as the rubber matrix.   Organosilicate intercalated by dimethyl, dihydrogenatedtallow, quaternary ammonium (Cloisite 15A, Southern Clay Products Inc., USA) with aspect ratio 75-100, was used in this work.   For comparison, conventional carbon black (CB, N-220, China Synthetic Rubber, Taiwan) and silica (Aerosil, Degussa, Germany) were also mixed with NBR in a two roll mixing mill directly. The composition used in this study is given in Table 3A-1.

The mixing of the organosilicate with elastomer was facilitated by the use of solvent [6, 26].   NBR was dissolved in methyl ethyl ketone (MEK).   The organosilicates were also swollen in MEK independently and then mixed with the NBR solution with vigorous stirring for 12hrs.   The MEK in the resulting dispersion was then evaporated and the sample dried under vacuum for 2 days.   After that, the resulting organosilicate-reinforced NBR was mixed with the additives and sulfur in a two-roll miller.   The samples were then cured at 160 ^{o}C in an electrically heated hydraulic press to their respective cure times, t_{90}.   These values were derived from a Monsanto oscillating disc rheometer (MDR 2000) - cf. Table 3A-2.

3-2.2 Characterization

Tensile and tear tests were performed on dumb-bell shaped specimens, following the ASTM standard D 412 and D 624, respectively on a material testing system machine (Sintech, MTS, USA) at a cross-head speed of 50 cm/min.   For each data point, five specimens were tested, and the average of the values was taken. Hardness was directly measured by hardnessmeter (Teclock, Japan) according to ASTM D 2240 standards.   Fourier-transformed infrared spectroscopy (FTIR) experiments were performed with a Perkin Elmer IR2000 spectrometer over a frequency range of 650-4000 cm^{-1}.   The samples for the FTIR study were prepared with cured   NBR compounds using compression moulding.   Thermogravimetric analysis (TGA) of each sample was carried out under nitrogen purge in a

Perkin-Elmer TGA-7.   About 10 mg of cured sample was heated from 50 to 750 ^{o}C

at 10 ^{o}C/min.   Dynamic-mechanical thermal analysis (DMA7, Perkin Elmer) spectra

were recorded on rectangular specimens (length x width x thickness = 6x 1x 0.25 cm^{3})

in tensile mode at a frequency of 10 Hz.   DMTA results, viz. storage modulus and

mechanical loss factor (tan δ) were measured in the temperature range from -100 to

70 ^{o}C at a heating rate of 5 ^{o}C /min.

The XRD patterns of the rubber samples were obtained by a D5000

diffractometer (Siemens, München, Germany) using Ni-filtered CuK$_{\alpha}$ radiation (λ =

0.1542 nm).   The samples were scanned in step mode at a 1.5 °/min scan rate in the

range of 2θ < 10°.   The TEM used is a JEOL JEM 2000FX electron microscope

operating with an acceleration voltage of 200 kV.   Ultrathin sections of the cured

samples were microtomed using Leica Ultracut Uct into about 100-nm thick slices

with a diamond knife; subsequently, a layer of carbon was deposited onto these slices

and placed on 400 mesh copper nets.   The crosslinking density of an elastomer can

be determined from equilibrium swelling or mechanical measurements.   Swelling

experiments were adopted in this thesis and carried out with cured samples by putting

the samples in toluene at 25 ^{o}C for 48 hrs in order to achieve the equilibrium swelling

condition.   The uptake solvent percentage, Q, and volume fraction of NBR in the

swollen gel, Vr, were calculated by the following equations:

$$Q = (M_{sw} - M_{i})/ M_{i} \qquad\qquad\qquad (1)$$

Where M_{i} and M_{sw} are the weight of the rubber sample before immersion in the

solvent and the swollen state, respectively.

$$Vr = (1/D_{sam}) / [(1/ D_{sam})+(Q/ D_{sol})] \qquad\qquad (2)$$

Where D_{sam} and D_{sol} are the densities of the rubber sample and solvent (0.87 for

toluene).   The crosslinking density of the sample,   , defined by the number of

elastically active chains per unit volume, was calculated by the Flory-Rehner equation

[27]:

$$\nu = -\frac{\ln(1-V_r) + V_r + \chi V_r^2}{V_s (V_r^{1/3} - V_r/2)} \qquad (3)$$

Where V_s is the molar volume of the swelling solvent (106.1 cm3/mol for toluene).

χ is the Flory-Huggins (rubber-toluene) interaction parameter and was taken as

0.435 for the NBR-toluene system in this calculation.

Crosslinking density has also been determined from equilibrium stress-strain

measurements using the Mooney-Rivlin equation :

$$\frac{\sigma}{2(\lambda - \lambda^{-2})} = C_1 + \frac{C_2}{\lambda} \qquad (4)$$

where σ is engineering stress, λ is extention ratio, C_1 and C_2 are constants. By

plotting $\sigma/[2(\lambda - \lambda^{-2})]$ versus $1/\lambda$ and extrapolating to $1/\lambda = 0$, a value of C_1 can be

obtained. By comparison with the theory of rubber elasticity, it has been proposed

that $C_1 = \frac{1}{2} NRT$, where N is crosslink density, R the gas constant, and T absolute

temperature.

Thermodynamical aspects of rubber elasticity are crucial to obtain a deeper

understanding of mixing in NBR/silicate nanocomposites. The expansion of rubber

in the presence of a solvent will significantly modify the conformational entropy (ΔS)

and the elastic Gibbs free energy (ΔG). The elastic Gibbs free energy can be

determined from the Flory-Huggins equation [11, 14]:

$$\Delta G = RT[\ln(1 - V_r) + V_r + \chi V_r^2] \qquad (4)$$

From the statistical theory of rubber elasticity, the conformational entropy ΔS can be

obtained from $\Delta G = -T \Delta S$, which assumes that no changes in the internal energy of

the network occurs upon stretching.

The water and solvent (methanol) vapor transmission were measured at 40 $^{\circ}$C and 50 % relative humidity, according to ASTM E96.   To minimize the influence of thickness on the vapor transmission, the thickness of the sample is set to be 5mm by molding.   The permeability, P, is calculated by the following equation:

$$P = 6237 \times (W\text{-}W_1) \tag{5}$$

Where W and W_1 are the weights of the sample assembly before and after testing respectively.   The relative permeability was defined as the measured permeability divided by the pure NBR permeability.

3-3   Results and Discussions

The dispersion image of layered silicates on the NBR matrix are shown and discussed in the section 2-3-A for the NBR-layered silicate nanocomposites.   The mechanical properties and the chemical reaction mechanism of the NBR-layered silicate nanocomposites are discussed in the section 2-3-B.

3-3-A.   Layered silicates dispersion in NBR nanocomposites

3-3-A.1   curing characteristics

Table 3A-1 gives the composition of NBR nanocomposites used in this study. Its curing characteristics are summarized in Table 3A-2.   In the presence of organosilicates, the initial scorch time, t_2, (about 89 seccond) was shorter than that of pure NBR (106 second).   This is because the acidic nature of organosilicate activates the formation of soluble zinc ions.   The soluble zinc ions in turn induces the decomposition of accelerator into free radicals in the earlier reaction stage.   These free radicals cause the premature vulcanization and result in a decrease of the scorch time.   The cure time of NBR nanocomposites, t_{90}, increased with the content of the organosilicate.   This result is different from the catalytic effect reported in some of

the NR/organosilicate nanocomposite literature [15]. It can be attributed to the

greater acidity of the organosilicates, which exhausts some decomposed accelerator

free radicals in the following crosslinking reaction, retarding curing and influences the

kinetics of the crosslinking reaction. Another possible cause [28] is resulted from

the ZnO, which neutralizes the most active sites of the filler surface and has been

proven in silica. Both M_L and M_H of these nanocomposites increase with the amount

of organosilicate, resulting an increase in the stiffness of NBR matrix effectively.

The increasing stiffness, M_H-M_L, corresponds with the increasing hardness tested

results as given in Table 3A-2.

3-3-A.2   *Dispersion of the silicates*

The efficiency of organosilicate in reinforcing the polymer matrix is primarily

determined by the degree of its dispersion in the matrix and the extent of intercalation

of organosilicate by polymer molecules. Figure 3A-1 shows the (001) diffraction

peak of the organosilicate is shifted to lower diffraction angles in the nanocomposite

as compared to that of the pure organosilicate. The d-spacings of the stacks were

3.53-4.26 nm for the NBR/organosilicate nanocomposites, whereas it is 3.15 nm for

the pure organosilicate. In the NBR nanocomposites containing 3 parts of layered

silicates has the largest interlayer distance, 4.26nm. At low silicate loading, the

viscosity of the nanocomposite is not large enough to generate a sufficient shearing

force for moving the majority of rubber molecules to intercalate into the layered

silicates gallery. Hence, the increase in the d-spacing of layered silicate is limited.

At high silicate loading, the dispersion of layered silicates is difficult, but a high shear

force has been resulted for moving large rubber molecules to intercalate into the

layered silicates gallery. Therefore, a compromise was reached by the two factors at

about 3 parts silicate loading. This indicates that an optimum loading of

organosilicate in the NBR case has been obtained. The peaks around 4.18-4.93° and

6.0-7.0^o result from higher order diffractions from the (002) and (003) diffraction planes, respectively.   The multi-diffraction peaks reflect a well-defined layered silicate structure.   In the case of 1 phr organosilicate in NBR, a lower but strong peak around 6.50^o (1.36nm) was displayed.   It has been attributed to the thermal degradation and desoption of the organic materials in the gallery [29].   In this study, however, the NBR nanocomposites were prepared by solution blending without a high temperature mixing process.   Thus, it is speculated to be an effect of the organosilicate confinement (reaggregation) [10, 15].   The formation of a zinc-sulfur accelerator complex "extracts" the amine intercalant of the organosilicates, thus causing the collapse of the layers.   Figure 3A-2 shows the TEM image of the NBR nanocomposite containing 7.5 phr organosilicate.   Most of the layered silicates are well-distributed in the NBR matrix and a large portion of the organic-modified silicate layer particles appear to be interlated along with a few single delaminated platelets. No visible differences in the morphology of any of the NBR/organosilicate samples can be found.   The TEM result is in consistent with that of the XRD study, as shown in Figure 3A-1.   Both TEM and XRD results thus confirm that the layers of the organosilicate particles have been intercalated successfully in the NBR nanocomposites.

3-3-B. Mechanical, thermal and barrier properties of NBR nanocomposites

3-3-B.1 Mechanical properties

Figure 3B-1 shows stress-strain curves in tensile for the NBR nanocomposites containing different amounts of organosilicate.   The tensile properties of these nanocomposites increase with the amount of organosilicate.   At high strains, stress hardening behavior is observed for the NBR incorporating organosilicate.   Table 3B-1 summarizes the ultimate properties of tensile strength, elongation at break,

modulus at 100, 300 and 500% elongation, and tear strength.   The mechanical

properties of the NBR nanocomposites, such as the tensile strength, elongation at

break, modulus at different elongation and tear strength relative to the pure NBR are

enhanced due to the presence of intercalated/exfoliated layered silicates.   A more

than six-fold increase in tensile strength, two-fold increase in M500, 39%

enhancement in elongation at break, and 267.8% enhancement in tear strength are

obtained with the addition of 10 phr of the exfoliated organosilicate.   These gains in

strength and stiffness without loss in elongation in these nanocomposites are quite

different from the behavior of conventional composites.   The reinforcing effect is

presumed to occur due to intercalated/exfoliated organosilicate layers that are covered

by highly crosslinked rubber molecular chains with strong interfacial interactions in

between [3, 9, 21].

Figure 3B-2 shows the tensile properties of NBR containing organosilicate, high

strengthening super abrasion furnace carbon black (CB, N220) and silica (Aerosil).

The reinforcing effect on NBR by organosilicate appears more pronounced.

Particularly, the reinforcing efficiency in the tensile modulus is higher than that of

NBR/CB compound under 600% strain.   For instance, only 3 to 5 parts of

organosilicate are enough to obtain a comparable tensile strength to that of NBR

containing 40 parts of Aerosil.   In the conventional carbon black, the reinforcing

effect was interpreted as bound rubber phenomenon involves physical adsorption,

chemisorption, and mechanical interaction [28].

Infrared spectra of the polymer nanocomposites can be used to illustrate the

occurrence of chemical reactions or strong interactions between polymer and

reinforcers [12, 21, 30-31].   Polymer/layered silicate nanocomposites are difficult to

analyze because of the reflective properties of the layered silicate platelets.   Figure

3B-3 shows FTIR spectra, over a frequency range of 950-1600 cm^{-1}, of organosilicate

as received, cured NBR/organosilicate and pure NBR compounds, Absorption peaks are observed at 1010, 1041, 1129 (C=S not linked to N), 1200 (C=S not linked to N), and 1242 (C=S linked to N) cm^{-1}, which are characteristic of cured pure NBR compound.　The peaks at 1010 and 1041 cm^{-1}, attributed to sulfoxide stretching vibrations, shift to 1040 and 1077 cm^{-1} in the NBR/organosilicate nanocomposite, due to the interferece effect of Si-O stretching vibrations in layered silicates.　The peaks at 1129, 1200, and 1242 cm^{-1}, attributed to the accelerator reaction products ((cyclohexyl benzthiazyl sulphonamide (CBS) and dibenzthiazyl disulphide (DM)) and sulfur, disappear in the NBR nanocomposite.　Whereas, a medium and broad absorption band at approximately 1217 cm^{-1} appears.　This indicates that a strong interaction between layered silicates and the curative reaction products exists and results in a new absorption peak in the NBR nanocomposite.　The interesting outcome is the appearance of a C-SO$_2$-N bond peak around 1365 cm^{-1} in the NBR nanocomposite, which is absent in the spectrum of pure NBR and of the layered silicates.　This may be the result of the possible reaction of an ammonium salt intercalant and zinc-sulfur-amine complexation between the organosilicate and highly polarized NBR during the vulcanization process.　Schematic drawings of the possible reaction mechanism are provided in Figure 3B-4.　NBR molecular chains were therefore more easily intercalated into the intergallery space of the organosilicate during this process.　Recalling the microstructure discussed above, the NBR molecules intercalated into the organosilicate layers could also be considered an effect of bound rubber.　This also indicates a strong interaction exists between the intercalated NBR chains and organosilicate layers [6].

　　　The effect of the incorporation of the organosilicate on the crosslinking density of NBR can be estimated by an application of the Flory-Rehner equation.　Table 3B-2 summarizes the crosslinking density and thermodynamical characteristics of the

NBR compounds.   The crosslinking density is found to increase with the amount of

organosilicates.   The crosslinking density for the NBR/organosilicate nanocomposite

is significantly higher than that of pure NBR.   The results are in agreement with

those vulcanization characteristics and the tensile properties, indicating a strong

rubber/organosilicate interaction (bound rubber) in the nanocomposites. Table 4 lists

the thermodynamical parameters,   G and   S, of the NBR nanocomposites.   A

considerable increase in the free energy is observed in the NBR/organosilicate

nanocomposites.   These results can be attributed to better compatibility between the

organosilicate and NBR rubber.   The NBR molecules can penetrate into the galleries

more easily and this results in intercalated/exfoliated structures.

3-3-B.2 Thermal properties and relaxation behavior

The thermal properties and relaxation behavior of NBR nanocomposites were

analyzed by TGA and DMA, respectively.   Table 3B-3 summarizes the degradation

temperatures (Td_5, Td_{50}), storage moduli (E'), glass transition temperatures (Tg), and

Tanδ values.   The degradation temperature at 5% and 50% weight loss were both

obtained in this study.   The Td_5 decreases with an increasing amount of

organosilicate. This is because the alkyl chain type organo-modifier, such as

hydrogenated tallow begins to decompose above 200 $^{\circ}$C [32].   Whereas, the

resistance of nitrile butadiene rubber molecules to thermal decomposition was

improved by the presence of intercalated/exfoliated organosilicate at temperature

higher than 450 $^{\circ}$C.   For instance, the decomposition temperature for a ten parts

loading of organosilicate on NBR nanocomposite (493 $^{\circ}$C) was 25 $^{\circ}$C higher than that

of pure NBR (468 $^{\circ}$C).

The onset storage modulus E', given in Table 3B-3, increases as the amount of

rganosilicate increases.   Specifically, the nanocomposites containing 10 phr

organosilicate have the highest storage moduli which are 57% higher than that of pure

NBR. These results can be attributed to the larger active surface area and stronger NBR/organosilicate interactions, which is in harmony with the mechanical results. The glass transition temperature was obtained from the peak temperature of tan δ as depicted in Table 3B-3. Decreases in Tg and tan δ also occur as the organosilicate content increases. Similar results were reported and rationalized for ammonium salt intercalated in silicate layers that may act as a plasticizer or lubricant [16, 32].

3-3-B.3 Barrier properties

Figure 3B-5 highlights the barrier improvement of NBR-based nanocomposites against water and methanol vapor. The relative vapor permeability of the NBR rubber is reduced markedly by 85% (from 100% to 15%) for water and by 42% (from 100% to 58%) for methanol, whereas the permeability values for water and methanol are 967 and 5111 $g/m^2/day$, respectively. This indicates the intercalated/exfoliated NBR/silicate nanocomposites improve the vapor barrier properties dramatically. It is noteworthy that the methanol permeability results agree with the crosslinking density results discussed above. Therefore, the permeability is controlled by the microstructure of the nanocomposite and the interaction between NBR and organosilicates.

The dramatic enhancement of mechanical properties of NBR by forming nanocomposites through a solution blending process presented in this study is attractive than those of NBR nanocomposites obtained by melt mixing or latex blending process as reported in the literature [18-20]. For example, a six folds increase in the tensile strength without a loss in the ultimate elongation by the solution method has been achieved. Whereas, a three to four folds increase of tensile strength is observed with a reduction in the elongation by conventional melt mixing process. Permeability test results show the same trends. This can be attributed to two factors. The first is that the interlayer distance of layered silicate was expanded more by the

solvation effect of MEK than by melt-mixing method.   The agglomerated silicate particles are reduced significantly by shearing force in the blending stage, which also lead to better dispersion and miscibility of organosilicate in NBR matrix.   Finally the large and coiled nitrile butadiene rubber molecular chains are also swollen and stretched in the good solvent, which is advantageous for intercalation during the blending process.

3-4   Conclusions

NBR/organosilicate nanocomposites, with exfoliated and intercalated structures, were successfully prepared by the solution blending method.   The hardness, tensile properties and tear strength of these nanocomposites increase substantially with the amount of incorporated organosilicates by containing a few weight percent of layered silicates, as compared to pure NBR.   This reinforcing effect can be attributed to strong interactions between the intercalated NBR molecular chains and organosilicate layers. Additionally, these nanocomposites exhibit higher thermal stabilities than those of pure NBR.   The relative vapor permeability of nanocomposites containing ten parts of layered silicates is reduced by 85% and 42% for water and for methanol, respectively, as compared to pure NBR.

Acknowledgements

References

[1] A. Usuki, M. Kawasum, Y. Kojima, Y. Fukushima, A. Okada, T. Kurauchi, and O. Kamigaito, *J. Mater. Res.,* **8**, 1179 (1993).

[2] M. Kawasumi, N. Hasegawa, M. Kato, A. Usuki, and A.Okada, *Macromolecules,* **30**, 6333 (1997).

[3] T. K. Chen, Y. I. Tien, and K. H. Wei, *Polymer,* **41**, 1345 (2000).

[4] H. L. Tyan, C. M. Leu, and K. H. Wei, *Chem. Mater.,* **13**, 222 (2001).

[5] P. C. LeBaron, Z. Wang, and T. J. Pinnavaia, *Appl. Clay Sci.,* **15**, 11 (1999).

[6] Y. T. Vu, J. E. Mark, L. H. Pham, and M. Engelhardt, *J. Appl. Polym. Sci.,* **82**, 1391 (2001).

[7] G. Unnikrishnan and S. Thomas, *J. Polym. Sci. Part B*, **35**, 725 (1997).

[8] K. S. Kwan, D. A. Harrington, P. A. Moore, J. R. Hahn, J. V. Degroot, and G.T. Burns, *Rubber Chem. Technol.,* **71**, 630 (2001).

[9] A. Mousa and J. Karger-Kocsis, *Macromol. Mater. Eng.,* **286**, 260 (2001).

[10] Z. Wang and T. J. Pinnavaia, *Chem. Mater.,* **10**, 3769 (1998).

[11] J. Karger-Kocsis and C. M. Wu,. *Polym. Eng. Sci.,* accepted in press (2004).

[12] S. Joly, G. Garnaud, R. Ollitrault, L. Bokobza, and J. E. Mark, *Chem. Mater.,* **14**, 4202 (2002).

[13] M. López-Manchado, B. Herrero, and M. Arroyo, *Polym. Int.,* **52**, 1070 (2003).

[14] M. Arroyo, M. López-Manchado, and B. Herrero, *Polymer*, **44**, 2447 (2003).

[15] S Varghese, J. Karger-Kocsis, and K. G. Gato, *Polymer*, 44, 3977 (2003).

[16] F. Schön, R. Thomann, and W. Gronski, *Macromol. Symp.,* **189**, 105 (2002).

[17] A. Usuki, A. Tukigase, and M. Kato, *Polymer,* **43**, 2185 (2002).

[18] W. G. Hwang, K. H. Wei, and C. M.Wu, *Polymer* accepted in revised (2004).

[19] J. T. Kim, T. S. Oh, and D. H. Lee *Polym. Int.,* **52**, 1203 (2003).

[20] C. W. Nah, H. J. Ryu, W. D. Kim, and S. S.Choi, *Polym. for Adv. Technol.,* **13**, 649 (2002).

[21] Y. I. Tien and K. H. Wei, *Macromolecules,* **34**, 9045 (2001).

[22] T. K. Chen, Y. I. Tien, and K. H. Wei, *J. Polym. Sci., Part A: Polym. Chem.,* **37**, 2225 (1999).

[23] Y. I. Tien and K. H. Wei, *J. Polym. Res.,* **7**, 245 (2000).

[24] S. D. Burnside and E. P.Giannelis, *Chem. Mater.,* **7,** 1597 (1995).

[25] P. C. LeBaron and T. J. Pinnavaia, *Chem. Mater.,* **13**. 3760 (2001).

[26] Y. I. Tien and K. H. Wei, *Polymer,* **42**, 3213 (2001).

[27] L. H. Sperling, *Introduction to physical polymer science*-2nd ed, chapt 9, p.382, copyright by John Wiley & Sons; New York (1993).

[28] M. Morton, editor, *Rubber technology*, New York: Van Nostrand Reinhold (1985).

[29] C. I. Park, O. O. Park, J. G. Lim, and H. J. Kim, *Polymer,* **42**, 7465 (2001).

[30] E. Passaglia, W. Bertuccelli, and F. Ciardelli, *Macromol. Symp*., **176**, 299 (2001).

[31] M. Pramanik, S. K. Srivastava, B. K. Samantaray, and A. K. Bhowmick, *J. Polym. Sci. Part B: Polym. Phys.,* **40**, 2065 (2002;).

[32] Y. S. Choi, M. H. Choi, K. H. Wang, S. O. Kim, Y. K. Kim, and I. J. Chung, *Macromolecules,* **34**, 8978 (2001;).

Table 3A-1 : Formulation of NBR compounds.

Material	phr
NBR	100
Organosilicate	0-10 (various)
ZnO	5
Stearic acid	2
Sulfur	1.5
Accelerators	2.2

phr: parts per hundred rubber

Table 3A-2 : Vulcanization characteristics of NBR compounds

Organosilicate content (phr)	t_2 (sec)	t_{90} (sec)	M_L (Lb-in)	M_H (Lb-in)	M_H-M_L (Nm)
0	106	382	0.40	5.48	5.06
1	88	383	0.40	5.60	5.20
3	87	409	0.41	5.62	5.21
5	89	412	0.45	6.26	5.81
7.5	91	412	0.57	6.44	5.87
10	87	412	0.67	6.85	6.18

t_2 : initial scorch time to 2 units of torque increase above
   minimum torque.

t_{90} : cure time to 90 % of maximum torque development.

M_L: minimum torque.

M_H: maximum equilibrium torque.

M_H-M_L: torque increase.
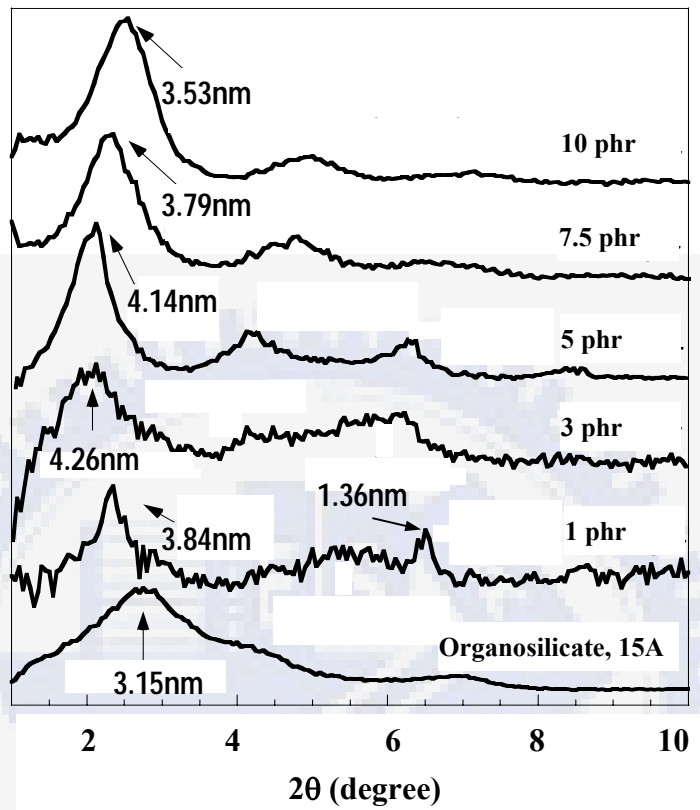
Figure 3A-1. X-ray diffraction patterns of NBR nanocomposites
with various organosilicate contents.
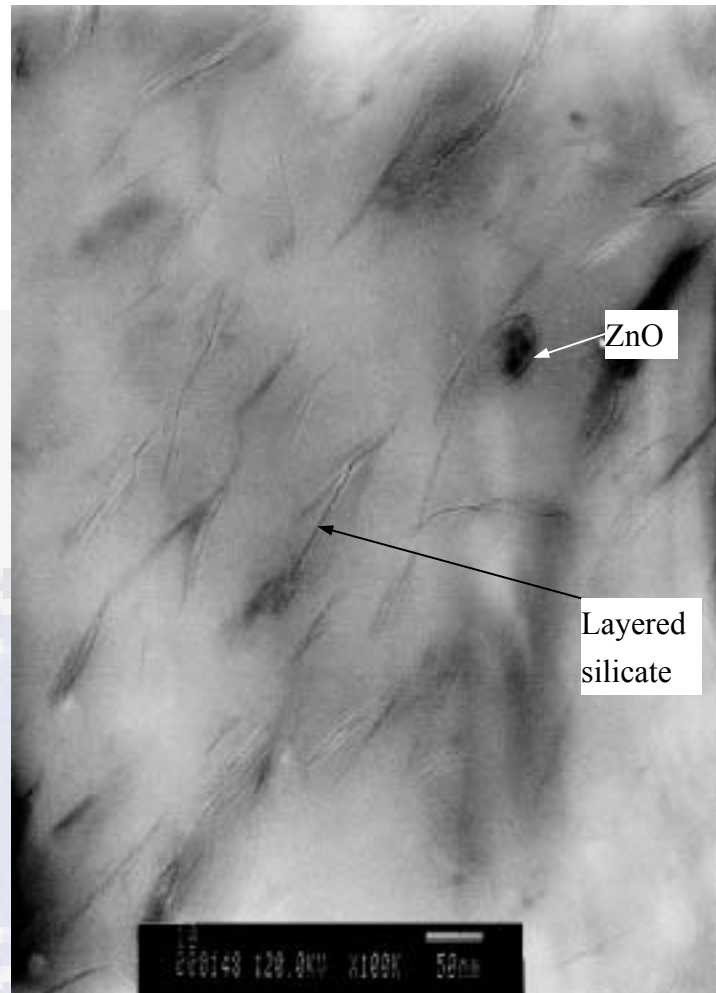
Figure 3A-2. TEM image taken on the NBR nanocomposite containing

7.5 phr organosilicates.

Table 3B-1 : Mechanical properties of NBR compounds

Organosilicate content (phr)	Hardness	Tensile strength (MPa)	Elongation at break (%)	M100 (MPa)
0	46	2.1 ±0.2	600 ±54	0.89 ±0.01
1	49	6.2 ±1.6	521 ±46	1.09 ±0.01
3	51	7.9 ±0.9	816 ±31	1.10 ±0.02
5	53	9.5 ±1.6	826 ±27	1.21 ±0.02
7.5	55	12.0 ±2.2	784 ±52	1.43 ±0.03
10	57	13.4 ±1.8	833 ±21	1.70 ±0.03

Organosilicate content (phr)	M300 (MPa)	M500 (MPa)	Tear strength (kg/cm)
0	1.24 ±0.03	1.73 ±0.07	8.7 ±0.1
1	1.51 ±0.03	2.02 ±0.07	11.6 ±1.0
3	1.64 ±0.04	2.25 ±0.07	14.2 ±0.6
5	1.81 ±0.03	2.45 ±0.07	15.3 ±0.6
7.5	2.42 ±0.10	3.59 ±0.21	19.8 ±0.5
10	2.70 ±0.09	3.85 ±0.13	23.3 ±0.1

M100: engineering modulus at 100% elongation.
M300: engineering modulus at 300% elongation.
M500: engineering modulus at 500% elongation.

Table 3B-2 : Crosslinking density and thermodynamical characteristics of NBR compounds.

Organosilicate content (phr)	Volume fraction	Crosslink density (mol /cm^3)	G (Jmol^{-1})	S (Jmol^{-1}K^{-1})
0	0.2518	1.995E-04	-26.96	8.899E-02
1	0.2485	1.927E-04	-25.99	8.579E-02
3	0.2547	2.055E-04	-27.83	9.186E-02
5	0.2532	2.024E-04	-27.38	9.035E-02
7.5	0.2687	2.366E-04	-32.32	1.067E-01
10	0.2759	2.538E-04	-34.81	1.149E-01

Table 3B-3 : Thermal properties of NBR compounds.

Organosilicate content (phr)	Td$_5$ (^{o}C)	Td$_{50}$ (^{o}C)	E' (×10^9 Pa)	Tg (^{o}C)	Tan δ (=E"/E')
0	403	468	1.98	-28	1.84
1	371	471	1.13	-25	1.73
3	355	479	1.88	-31	1.78
5	344	477	2.06	-28	1.60
7.5	340	487	2.33	-32	1.55
10	337	493	3.11	-31	1.34

Td$_5$ (^{o}C): degradation temperature at 5% weight loss.

Td$_{50}$ (^{o}C): degradation temperature at 50% weight loss.
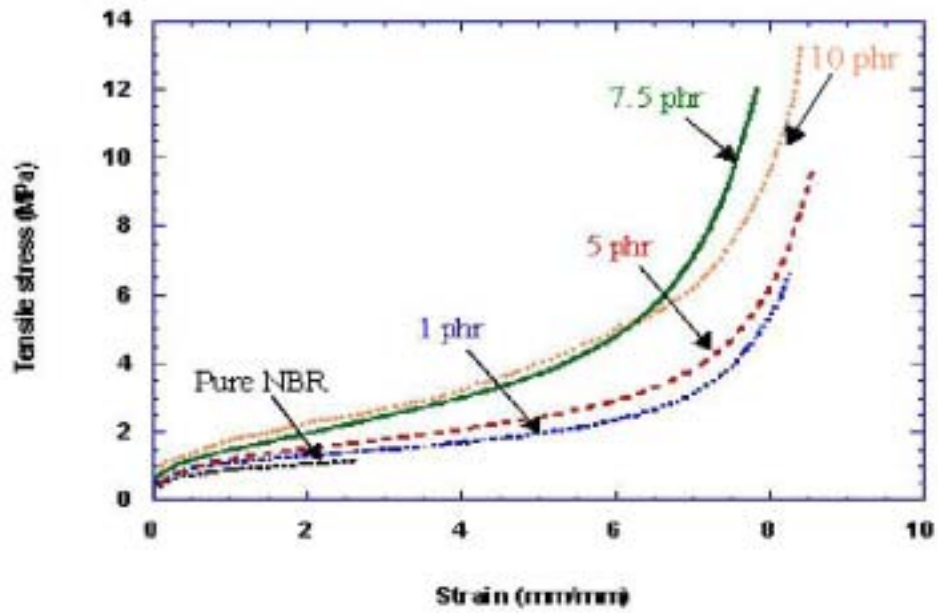
Figure 3B-1. Typical tensile stress/strain curves of the NBR nanocomposites

with various organosilicate content.
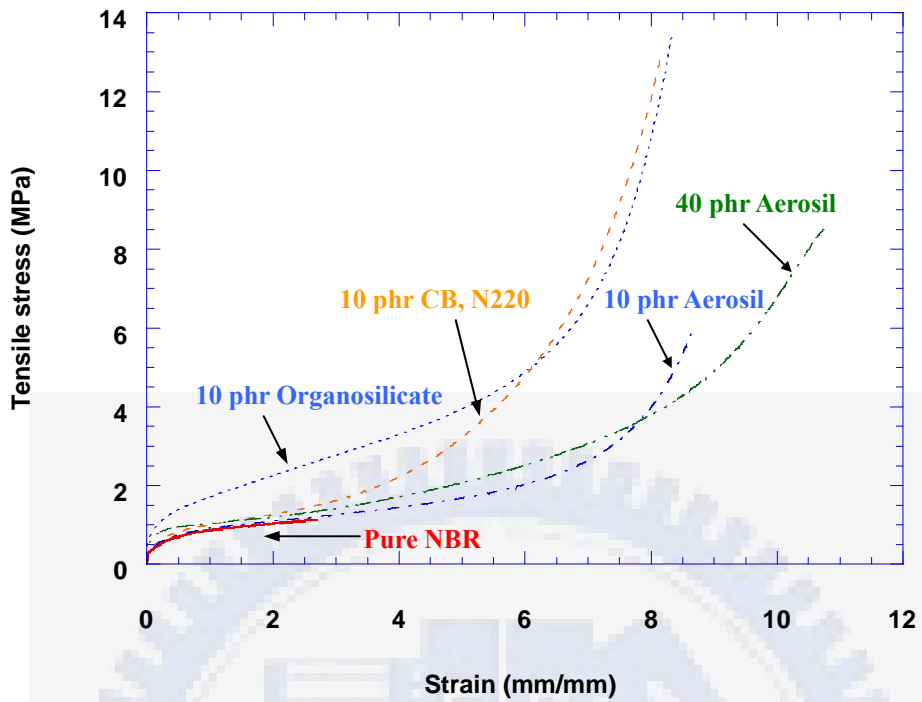
Figure 3B-2. Typical tensile stress/strain curves demonstrate the reinforcing

effect in NBR/organosilicate nanocomposites.
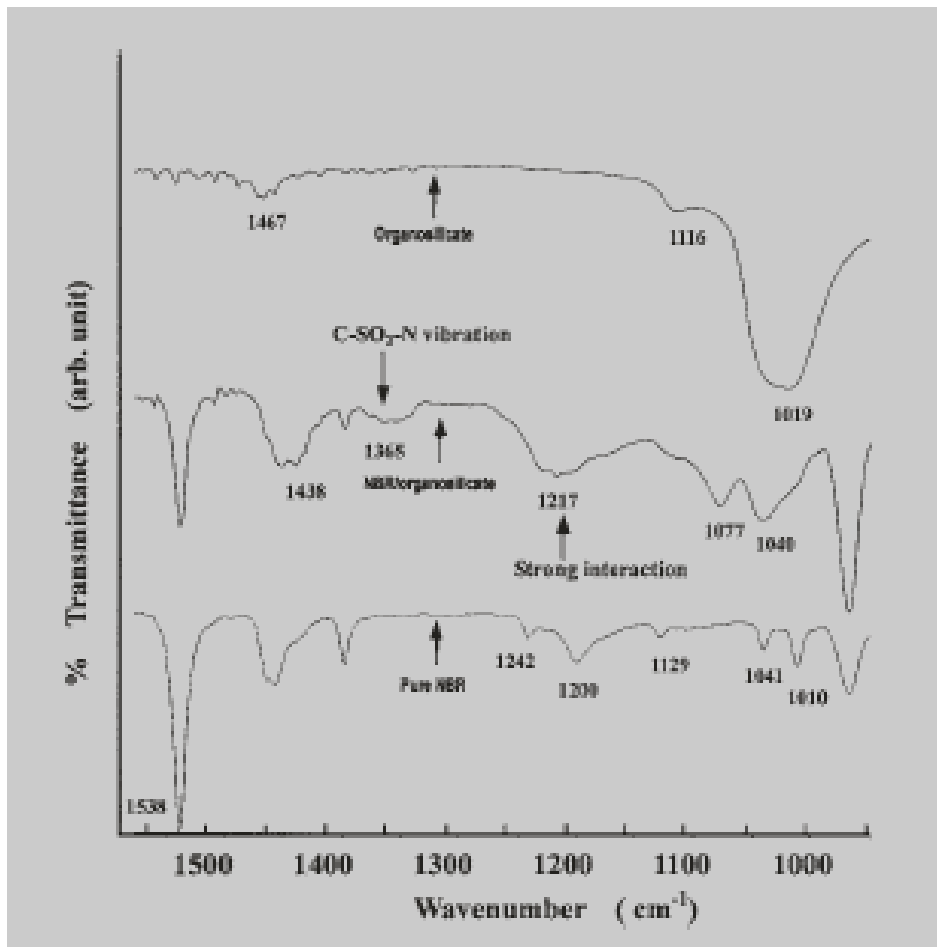
Figure 3B-3. FTIR spectra of organosilicate, NBR nanocomposite

(10 wt% organosilicate) and pure NBR.

Reaction mechanism

1. $ZnO + RCOOH \rightarrow Zn^{++}(RCOO)^-_2$ $\xrightarrow{\text{accelerator R-S-S-R}'}$ $R\text{-}S$ $+ R'\text{-}S$
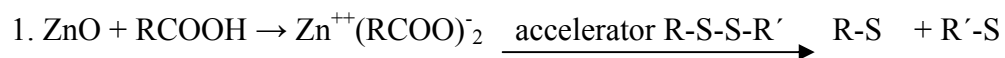
2. Acceleration of CBS :
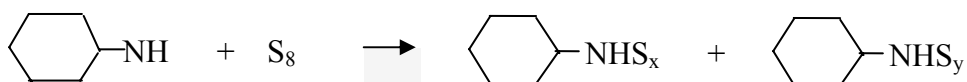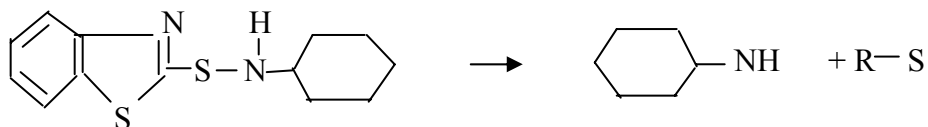
3. Vulcanization

4. Intercalation

layered silicate

organomodifier

NBR molecular chain
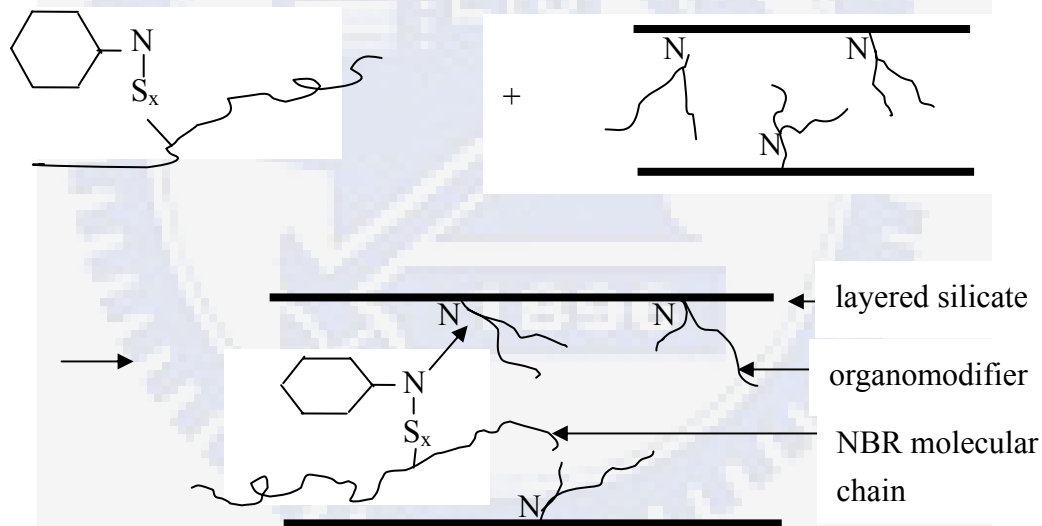
Exfoliation and intercalation morphology

Figure 3B-4. Possible reaction mechanism of ammonium salt intercalant and

zinc-sulfur-amine complexation between organosilicate and highly

polarized NBR.
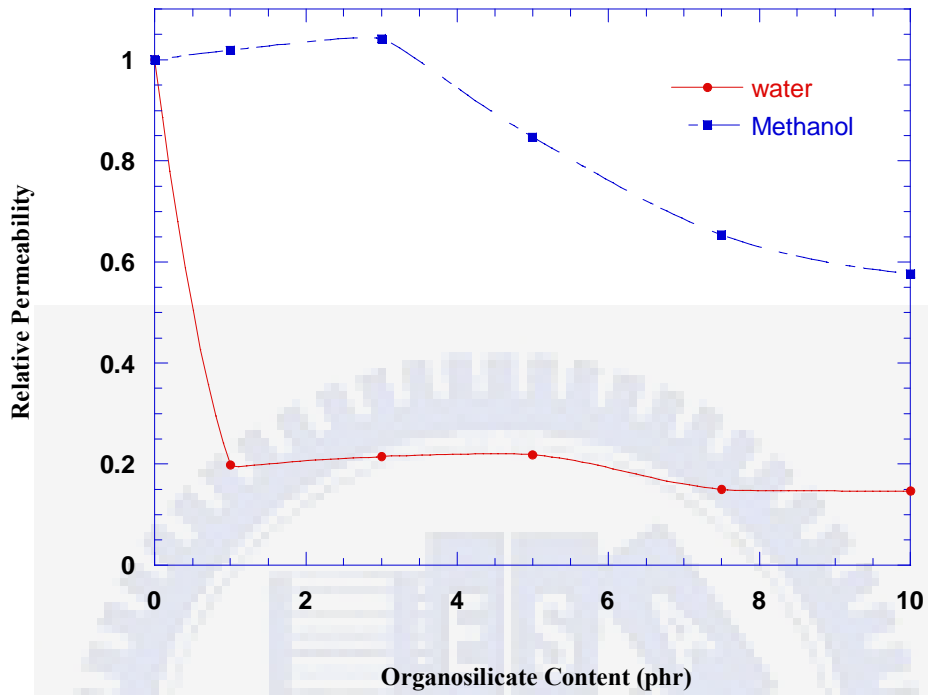
Figure 3B-5. Relative vapor permeability of NBR nanocomposites containing various amounts of organosilicate. Note: The reference values for water and methanol are 967 and 5111 $g/m^2/day$, respectively.

Chapter 4: Synergistic Effect of Compatibilizer in Layered Silicate Reinforced BR Nanocomposites

4-1 Introduction

Polymer nanocomposites based on the reinforcing of silicate layers derived from montmorillonite and thermoplastic or thermosetting polymers have been developed extensively over the past decade [1–5]. These materials have been predicted to provide superior mechanical strength, stiffness, thermal stability, and barrier properties, even when using only a very low weight percentage of montmorillonite [6–9]. Typically, an intercalated or exfoliated structure of the layered silicate can be obtained in the host polymer. Intercalated layered silicates possess a slightly increased intergallery space, which appears as an intense peak at a lower X-ray diffraction angle, and they retain their same orientation in the polymer matrix. In contrast, exfoliated silicates exist as monolayer silicates that become completely separated from one another in the polymer matrix; they are characterized by the absence of intense peaks in their XRD patterns, as well as through TEM observations.

Several methods have been developed for the effective preparation of intercalated or exfoliated layered silicate reinforced nanocomposites of nylon, polyimide, epoxy, polysiloxane, acrylonitrile butadiene rubber (NBR), SBR, polyurethane matrixes, and the other polymer systems [1–23]. These methods include in situ polymerization of monomers [7, 10–13], melt blending [14–18], emulsion polymerization or latex blending [19, 20], and solution blending using polar organic solvents [21–23]. In most cases, suitable chemical treatment and optimized processing are both keys to the successful formation of the

nanocomposites.   In our laboratory, we have obtained some nanocomposites that have potential for application in the electronics and dipped goods industries [7, 12, 19].

To obtain exfoliated nanocomposites, it is necessary to select amphiphilic molecules to modify the layered silicates, expand the intergallery space, and interact suitably with the molecules in the matrix.   One end of the amphiphilic molecule may be, for example, a hydrophilic quaternary alkylammonium ion unit for interacting with the silicates, while the other end may have hydrophobic groups or chemically reactive functional groups that can be either compatible with or covalently bonded to the polymer, thereby increasing the miscibility of the silicates and the polymers [4, 24].   A suitable compatibilizing component can be used to increase the interaction of two originally immiscible surfaces through hydrogen bonds, to avoid phase separation, and to prevent interfacial failure [25–30]. Polarity is the other significant factor to be considered when preparing a successful polymer nanocomposite.   Organo-modified layered silicates having high polarity and largely expanded d-spacing are relatively easier to intercalate with a highly polar polymer when using a method such as shear blending, but they are not miscible with nonpolar polymers.   Preparing a miscible and well-intercalated nanocomposite from a nonpolar polymer and a polar organosilicate usually requires a compatibilizer to act as a surfactant.

Carbon black and silica are the two most effective rubber reinforcing agents. In contrast, only a few studies have been reported on the use of organosilicates to reinforce rubber.   For a conventional filling effect, the main factors that cause significant reinforcement are a high specific area, the nature of the structure, and the surface chemistry.   The reinforcing effect of rubber nanocomposites containing just a few weight percent of layered silicates is similar to that of rubber compounds

having much higher loadings of silica or carbon black [15, 31, 32].   The efficiency of the silicates in modifying the properties of the rubber is largely determined by their degree of dispersion and the extent of their exfoliation in the rubber. Polyolefinic rubbers are more hydrophobic than are a number of thermoplastics and, therefore, it is necessary to process the layered silicates properly to achieve good dispersion.   In addition, the very high viscosity of molten rubber due to its high molecular weight can generate high shear stresses locally during compounding, and cause the peeling apart of layered silicate stacks.   Therefore, the layered silicates will be much easier to be delaminated [33, 34].   In this study, we used a two-stage compounding procedure—high-shear-force blending in a Banbury mixer at room temperature followed by hot melt blending at 150 °C—along with the use of a selected compatibilizer to obtain the intercalated/delaminated rubber nanocomposites.

To obtain a more detailed expression on the reinforcing effect of the organosilicate in rubber, we selected a nonpolar BR and a hydrophobic organosilicate to produce the nanocomposites through a two-stage melt blending method.   Because BR is one of the most important industrial raw materials whose reinforcement has only a fewer to be reported [30, 35], we believed that such a study would be of great importance.   In this study, we examined the effect that the amount of organosilicate has on the mechanical, thermal, and barrier properties of the resulting nanocomposites.   In addition, we also studied the thermodynamic behavior of these nanocomposites.

4-2 Experimental Methods and Analysis

4-2.1 Material preparation

Butadiene rubber (Taipol, BR, 0150, Taiwan Synthetic Rubber Co. Inc., Taiwan, R.O.C.), a conventional nonpolar material that has poor green strength and

tear strength, was selected as the rubber matrix.   Nanomer I.28E, an organosilicate modified by quaternary trimethylstearylammonium ions having an approximate aspect ratio of 75–120, was purchased from Nanocor Co. Inc., USA.   The compatibilizers used in this study—carboxylated terminated butadiene oligomer (CTB) and carboxylated terminated butadiene acrylonitrile copolymer (CTBN) having a molecular weight of ca. 3000–4000 g/mol—were obtained from Aldrich Chemical Co. Inc., USA.   Different contents of the layered silicates and compatibilizer were added to BR; they are named BR-0 (neat BR), BR-5 (BR having a loading of 5 wt% of layered silicates), and BR-5-7.5 (BR having a loading of 5 wt% layered silicates and a 7.5% weight ratio of CTB to the layered silicates). Typical industrial formulations were used (Table 4A-1).

4.-2.2 Process design

The compounds of rubber/organosilicate nanocomposites were prepared in a 3-L Banbury mixer using a two-stage process.   The first stage of the two-stage process involved blending the rubber, organosilicate, compatibilizer, and any other additives at room temperature in a Banbury mixer with the degree of fill at 80% and a rotation speed of 60 rpm for 8 min, then adding zinc oxide and blending again for 2 min before dropping down.   The second stage involved re-blending the compounds at 150 °C in the mixer for 4 min with the similar mixing condition as the first stage, dropping down the compounds, then by adding the cure agents at room temperature on a two-mill roller.   After aging at room temperature for 24 h, the samples were cured at 160 °C in an electrically heated hydraulic press to their respective cure times, t_{90}.   These values were derived from a Monsanto oscillating disc rheometer (MDR 2000) - cf. Table 4A-2.   Then, the test specimens were prepared.

4-2.3 Characterization

Tensile and tear tests were performed on a material testing system machine (Sintech, MTS, USA) at a cross-head speed of 50 cm/min, according to the ASTM standards D 412 and D 624, respectively. For each data point, five specimens were tested, and the average of the values was obtained. Thermogravimetric analysis (TGA) of each sample was performed under a nitrogen purge in a Perkin-Elmer TGA-7 instrument. The cured sample (ca. 10 mg) was heated from 50 to 750 °C at a rate of 10 °C/min. Dynamic mechanical thermal analysis (DMA7, Perkin–Elmer) spectra were recorded using 6-cm-long, 1-cm-wide, and 0.25-cm-thick rectangular specimens in the tensile mode at a frequency of 10 Hz. DMTA spectra, viz. the storage modulus and mechanical loss factor (tan δ), were measured over the temperature range from –100 to 70 °C at a heating rate of 5 °C/min.

Wide-angle X-ray diffraction (XRD) patterns of the rubber samples were obtained using a D5000 diffractometer (Siemens, Munich, Germany) and Ni-filtered CuK$_\alpha$ radiation (λ = 0.1542 nm). The samples were scanned in the step mode at a scan rate of 1.5°/min in the range $2\theta < 10°$. Transmission electron microscopy (TEM) measurements were performed using a JEOL JEM 2000FX electron microscope operating at an acceleration voltage of 200 kV. Ultrathin sections of the cured samples were microtomed, using a Leica Ultracut Uct and a diamond knife, into ca. 100-nm-thick slices; subsequently, a layer of carbon was deposited onto these slices and then they were placed onto 400-mesh copper nets. Field emission scanning electron microscopy (FE-SEM) images were obtained using a JEOL JSM-6340F electron microscope operating at an acceleration voltage of 5 kV and 12.5 μA. A layer of gold was deposited onto the inspected section of the cured samples using a JFC-1200 fine-coater. The water vapor permeability was measured using a Mocon PERMATRAN-W 3/60 instrument at 40 °C and 90% relative humidity of water.

The crosslinking density was determined by performing equilibrium swelling

as described in a previous report [31].   Swelling experiments were performed with

the cured samples by equilibrating them in toluene at 25 °C for 48 h.   The uptake

solvent percentage, Q, and volume fraction of BR in the swollen gel, Vr, were

calculated using the following equations:

$$Q = (M_{sw} - M_i)/ M_i \qquad (1)$$

where M_i and M_{sw} are the weights of the rubber sample before immersion in the

solvent and in its swollen state, respectively.

$$Vr = (1/D_{sam})/[(1/D_{sam}) + (Q/D_{sol})] \qquad (2)$$

where D_{sam} and D_{sol} are the densities of the rubber sample and solvent, respectively

(0.87 for toluene).   The crosslinking density of the sample,   , defined by the

number of elastically active chains per unit volume, was calculated by applying the

Flory–Rehner equation [36]:

$$= - \frac{\ln (1\text{-}Vr) + Vr + \quad Vr^2}{Vs (Vr^{1/3} \quad Vr/2)} \qquad (3)$$

where Vs is the molar volume of the swelling solvent (106.1 cm^3/mol for toluene)

and   is the Flory–Huggins (rubber–toluene) interaction parameter, which was

taken to be 0.38 for the BR–toluene system.   Determining the thermodynamic

aspects of the rubber elasticity is crucial for obtaining a deeper understanding of the

mixing in the BR/silicate nanocomposites.   The expansion of rubber in the

presence of a solvent will significantly modify the conformational entropy (S) and

the elastic Gibbs free energy (G).   The elastic Gibbs free energy can be

determined from the Flory–Huggins equation [9, 14]:

$$G = RT[\ln(1 - Vr) + Vr + \quad Vr^2] \qquad (4)$$

From the statistical theory of rubber elasticity, the conformational entropy   S can

be obtained from the equation $\Delta G = -T \Delta S$, which assumes that no changes in the

internal energy of the network occur upon stretching.

4-3 Results and Discussions

To distribute and disperse the high polar organo-modified layered silicates well

into the nonpolar BR rubber matrix are considerably difficult.   It needs some

compatibilizers or surfactants to act as an interlocker to connect both interfaces of

the silicates and the BR rubber to enhance the mechanical properties of the

nanocomposites.   The dispersion image of layered silicates on the BR matrix will

be shown and discussed in the section 4-3-A for the BR-layered silicate

nanocomposites with or without the compatibilizers.   The mechanical, thermal, and

the barrier properties of the BR-layered silicate nanocomposites are also discussed

in the section 4-3-B.

4-3-A. Layered silicates dispersion in BR nanocomposites

4-3-A.1 Vulcanization characteristics

Table 4A-2 lists the representative vulcanization characteristics of BR

nanocomposites containing 10 phr organosilicate and different amounts of

compatibilizer.   In the presence of organosilicates, the initial scorch time, t_2, was

shorter than that of neat BR (81 vs. 169 s).   This phenomenon occurred because the

acidic nature of the organosilicate activates the formation of soluble zinc ions, which

in turn induces the decomposition of the accelerator into free radicals in an earlier

stage of the reaction.   These free radicals cause the premature vulcanization, which

results in a decrease of the scorch time.   The cure time, t_{90}, behaves in a manner

similar to that of the t_2; this behavior is caused by a catalytic effect that has been

reported previously [9].   Some accelerator free radicals for crosslinking can react

with the compatibilizer and, therefore, retard the curing time. The values of both M_L and M_H of these nanocomposites increase upon the addition of the organosilicate at a low concentration; these increases result in an increase in the stiffness of the BR matrix based on the same curing system, but a decrease when the amount of compatibilizer increases. The increasing stiffness, $M_H - M_L$, follows the same trend as does the value of M_H.

4-3-A.2 Distribution and dispersion morphologies of the silicates

The efficiency of the organosilicate in reinforcing the polymer matrix is determined primarily by the degree of its dispersion in the matrix and by the extent in which the polymer molecules intercalate in the organosilicate. Figure 4A-1 provides the XRD patterns of the representative BR nanocomposites containing 5 phr of organosilicate and various amounts of CTB. The pure organosilicate displays two independent diffraction peaks, denoted (001, A) and (001, B), having values of 2θ ca. 3.51° ($d_{001, A} = 2.52$ nm) and 5.43° ($d_{001, B} = 1.63$ nm), respectively. The BR/organosilicate nanocomposites also display two independent diffraction peaks due to the addition of the organosilicate. The largest intercalated intergallery distance of these BR/organosilicate nanocomposites is much higher than that of the pure organosilicate ($d_{001, A} = 2.52$ nm). Table 4A-3 lists the complete X-ray diffraction data of the BR/organosilicate nanocomposites. The lowest diffraction peak of these nanocomposites, denoted (001, A), has values of 2θ between 1.2 and 1.8° ($d_{001, A} = 4.77–7.07$ nm). Another independent diffraction plane, denoted (001, B), has values of 2θ between 2.1 and 2.2° ($d_{001, B} = 4.01–4.21$ nm). The very clear multi-diffraction peaks at ca. 4.2 and 6.5°, which result from higher-order diffraction, reflect the well-defined layered silicate structure. This observation indicates that at a proper silicate loading and using a suitable mixing process, the viscosity of the

nanocomposite can be large enough to generate a sufficient shearing force to further

separate the intercalated silicate layers and to allow the rubber molecules to diffuse

into the intergalleries, where the compatibilizers are miscible with the rubber

molecules.   As a result, the d-spacing of the layered silicate is expanded sufficiently.

In the case of the 5 phr organosilicate in BR, a lower, but strong, peak appeared at ca.

6.5° (1.36 nm); this signal has been attributed to the thermal degradation and

desorption of the organic materials in the gallery [37] or to an effect of the

organosilicate confinement (re-aggregation) [9, 14, 31].   The formation of a

zinc–sulfur accelerator complex "extracts" the amine intercalant of the

organosilicates, which, thus, causes the collapse of the layers.

   Figure 4A-2 displays a TEM image of the BR nanocomposite containing 10 phr

organosilicate and 3 phr CTB compatibilizer.   Most of the layered silicates are

dispersed well in the BR matrix, and a large portion of the organic-modified silicate

layer particles appear to be intercalated along with a few single delaminated platelets.

No visible differences appear in the morphology of the BR/organosilicate

nanocomposites.   Figure 4A-3 presents an enlarged TEM image.   It is apparent

that there are ca. four to seven layers of single intercalated platelets that have an

intergallery distance of ca. 6 nm.   Figure 4A-3 indicates that the layered silicate

bundles exist in the BR/organosilicate nanocomposite, which suggests an

intercalated tactoids morphology.   The results of TEM analysis are in consistent

with those of an XRD study (Table 4A-3).   Thus, the TEM and XRD results both

confirm that the layers of the organosilicate particles have become intercalated in the

BR nanocomposites and that the structures of the organosilicate platelets can be

described as intercalated tactoids.   At a high silicate loading, dispersion of layered

silicates becomes difficult, but the high shear force applied causes the large rubber

molecules to intercalate into the gallery of the layered silicates.   This process may

primarily contribute to the synergistic effect of the proper shear force and the wetting effect of the compatibilizer between the BR molecular chains and layered silicates. The well-understood wetting effect would result in the BR rubber molecule chains migrating or transporting into the largely expanded intergallery spaces of the layered silicates.

The influence that the compatibilizer has on the morphology of the BR/organosilicate nanocomposites can be visualized from the fractured surface. Compatibilizers usually act as wetting agents—improving the surface energy of both immiscible phases—that become entangled or interlocked with the bulk chains at the interface between the two incompatible components. It is sometimes necessary to connect a ductile rubber with a semi-rigid filler in a mechanical blending system through suitable selection of a compatibilizer, which increases the mechanical strength of the interface by allowing stress transfer to occur across it [25-26, 28–30]. In our present system, which differs from that of a highly polar NBR [31], the compatibilizing effect is the dominant factor when the nonpolar BR incorporates the polar-structured organosilicates. Figures 4A-4 and 4A-5 display FE-SEM images of the fracture surfaces of the BR/organosilicate nanocomposites containing and lacking the compatibilizer, respectively. In Figure 4A- 4, we clearly observe a relatively uniform and tight fractured surface of the BR nanocomposite containing the compatibilizer; the well-dispersed layered silicates are enclosed by the matrix and interlocked into the matrix phase. Very few voids, holes, and crack defects are present and no visible phase separation or craze propagation. In contrast, the fracture interface of the BR nanocomposite in the absence of the compatibilizer indicates that both phases possess relatively loose and phase-separated structures. In this image, we observe many cracks and voids and a crinkly disordered interface. From the FE-SEM and TEM results, we conclude that the blending of a polar

organosilicate directly with a nonpolar BR must involve a compatibilizer as well as
suitable process parameters if it is to generate a reinforced rubber nanocomposite
containing well-dispersed layered silicates.

4-3-B. Mechanical, thermal and barrier properties of BR nanocomposites

4-3-B.1 Mechanical properties

Figure 4B-1 presents the tensile stress–strain curves for BR nanocomposites
containing different amounts of organosilicate and in the presence and absence of
the compatibilizer.   It is apparent that the BR nanocomposite displays the highest
tensile strength and elongation when it incorporates both the organosilicates and the
compatibilizers.   In contrast, the nanocomposite containing only the organosilicate
has relatively improved tensile strength and elongation than that of the neat BR.
The nonpolar BR, which has a low surface energy, is not very compatible with the
polar organosilicate.   An amphiphilic compatibilizer having a structure similar to
that of BR, but also having some polarity, is most suited to enhancing the wettability
and the interfacial interactions between the BR and the organosilicate.   CTB, an
oligomer that has both a slight polarity and a structure similar to that of BR, can
move more rapidly into the intergallery spaces of the layered silicates than can the
BR molecular chains, which leads to the entrance also of the intercalated BR
molecular chains.   We have found, however, that the BR nanocomposite containing
both the organosilicate and the CTBN oligomer compatibilizer enhances the
mechanical properties to a degree similar to that of the nanocomposite incorporating
only the organosilicate.   This finding may be due to the highly polar CTBN not
being miscible with the nonpolar molecular chains of BR, which in turn reduces the
interfacial interaction between the BR and the organosilicate, which even causes
similar phase separation phenomena to those presented in Figure 4A-5.   This

phenomenon can be more easily understood as that of a conventional plasticizer, which softens the matrix but reduces the tensile strength.   The tear strengths presented in Figure 4B-2 follow the same trends as that of the tensile properties of those nanocomposites.   We obtained significant improvements in the mechanical strength of the BR nanocomposites by using the melt blending method, followed by a vulcanization process, with the addition of a suitable compatibilizer.   These results correspond to those observed in the FE-SEM images.

The mechanical properties of these nanocomposites increase upon increasing the amount of organosilicate and the relative loading ratio of CTB to organosilicate. Figures 4B-3 and 4B-4 display the materials' tensile strengths and tear strengths. The mechanical properties of the BR nanocomposites are enhanced relative to those of the neat BR because of the presence of the intercalated/exfoliated layered silicates. We obtained a more-than-four-fold increase in the tensile strength, a 150% increase in modulus at 100% elongation (M100), and 232 and 410% enhancements in the tear strength and elongation at break, respectively, upon the addition of 10 phr organosilicate and 3 phr CTB, relative to the corresponding values of neat BR.   The enhancment in the mechanical properties and the gains in the elongation of these nanocomposites are quite different from those of conventional composites.   The reinforcing effect is presumed to occur as a result of the intercalated/exfoliated organosilicate layers being covered by highly crosslinked elastomer molecular chains with a strong interfacial interaction between them [5, 13, 19].   The other effect may be the result of possible reactions of the ammonium salt intercalant and the zinc–sulfur–amine complex occurring between the organosilicate and BR during the vulcanization process; we have provided and discussed a similar reaction mechanism in a previous publication [31].   As a result, the BR molecular chains are

more easily intercalated into the intergallery space of the organosilicate during this process.

We have also found that the mechanical properties improve upon increasing the loading ratio of CTB to organosilicate when it is below 30%, which is probably the upper limit of the loading ratio necessary to prepare intercalated/exfoliated elastomeric nanocomposites possessing outstanding mechanical properties.   When the ratio increases above 30%, the mechanical properties decrease slightly.

The effect that the incorporation of the organosilicate has on the crosslinking density of BR can be estimated by using the Flory–Rehner equation.   Table 4B-1 summarizes the crosslinking density and thermodynamical characteristics of the BR compounds.   The BR nanocomposites containing compatibilizers display higher crosslinking densities than do the other BR compounds.   The crosslink density and the thermodynamic characteristics both reach plateaus at high CTB loadings, which indicates that exhausting of the cure agent by the compatibilizer occurs and leads to a slight decrease in the crosslink density.   These results are in agreement with those of the vulcanization characteristics and the tensile properties and indicate that a strong rubber/organosilicate interaction occurs in the nanocomposites.   Table 4B-1 lists the thermodynamic parameters, ΔG and ΔS, of the BR nanocomposites. We observe a relative increase in the free energy of the compatible BR/organosilicate nanocomposites, which we attribute to the improved compatibility among the BR, compatibilizer, and organosilicate phases.   Therefore, the molecular chains of the BR can penetrate into the galleries more easily to result in an intercalated/exfoliated structure.

4-3-B.2 Thermal properties and relaxation behavior

We analyzed the thermal properties of the BR nanocomposites by using TGA. Table 4B-2 summarizes the values of the degradation temperatures (Td).   The

5%-weight-loss temperature decreased upon increasing the amount of organosilicate. This situation arose because the organo-modifier begins to decompose at temperatures above 200 °C [20].   We chose the temperature at which 50% weight loss occurred to be the degradation temperature.   As expected, the resistance to thermal decomposition improved upon the addition of the organosilicate, but it became weaker upon the addition of the low-molecular-weight CTB.   The decomposition temperature of the nanocomposite containing a 10 phr loading of organosilicate (561 °C) was 51 °C higher than that of neat BR (510 °C), but it increased only slightly (9–13 °C) upon the addition of CTB.

The relaxation behavior of the nanococomposites is investigated by using DMA. The values of storage moduli (E´), glass transition temperatures (Tg), and tan δ are also summarized in Table 4B-2.   The onset storage modulus (E´) of the nanocomposite increased more with respect to the amount of organosilicate and the CTB-to-organosilicate loading ratio than did that of the neat BR.   These results can be attributed to the larger active surface area and stronger BR–CTB–organosilicate interactions, and are consistent with the results of their mechanical properties (referred to Figure 4B-3), especially related to the tensile modulus (e. g., M100) from tensile test.   We obtained the glass transition temperature from the peak temperature of tan δ, as depicted in Table 4B-2.   Greater decreases in the values of Tg and tan δ—relative to those of the neat BR—also occurred as the organosilicate content increased.   Similar results have been reported and rationalized for ammonium salts intercalated in silicate layers that may act as plasticizers or lubricants [19, 38].   When a compatibilizer is added, well-intercalated BR molecular chains can be led into the intergallery space of the layered silicate more readily and constructed more tightly; this process may constrain the mobility and flexibility of the alkylammonium salt and also result in increases in the values of the

decomposition temperatures (5% weight loss), storage moduli (E´), glass transition

temperatures (Tg), and tan δ.

4-3-B.3 Barrier properties

Figure 4B-5 displays the improvement in the barrier to water vapor of the

BR-based nanocomposites.   The relative water vapor permeability of the BR

nanocomposites reduced markedly (by 80%: from 100 to 20%); the permeability

value for water in neat BR is 50.51 gm/m^2·day.   This finding indicates that the

intercalated/exfoliated BR/silicate nanocomposites improve the vapor barrier

properties dramatically.   The permeability is controlled by the microstructure of the

nanocomposite and by the interactions between the BR and the organosilicates.   It

seems that the compatibilizer has little effect on the water vapor permeability of the

BR nanocomposites.

The dramatic enhancements we present in this study of the mechanical

properties of the BR after forming nanocomposites through a two-stage melt

blending process are quite attractive when compared to those of other rubber

nanocomposites obtained when using the latex blending or solution or melt mixing

processes that have reported in the literature [19, 31, 38-39].   For example, using

this method we have achieved a fourfold increase in the tensile strength and the

ultimate elongation.   The thermal properties and the results of permeability tests

indicate the same positive trends, which can be attributed to a number of factors.

The first is that the interlayer distance of the layered silicate is expanded more by

the CTB compatibilizer and a synergistic effect leads to better compatibility among

the BR, compatibilizer, and organosilicate phases.   Therefore, the BR molecular

chains can penetrate into the galleries more readily and result in an

intercalated/exfoliated structure [26, 30].   In addition, the number of agglomerated

silicate particles is reduced significantly by the shearing force present during melt

blending when using a suitable compatibilizer; this process also leads to the better dispersion and miscibility of the organosilicate in BR matrix.

4-4 Conclusions

We have successfully prepared BR/organosilicate nanocomposites that have intercalated and partially exfoliated structures by using a two-stage melt blending method. As a result of counteracting the polarity effect and compatibility effect, the tensile properties and tear strengths of these nanocomposites increase substantially—relative to those of the neat BR—upon increasing the amounts of incorporated compatibilizer and organosilicates that contain a low weight percent of layered silicates. These results are attributed to the significantly improved compatibility and the strong interactions among the polar layered silicates, compatibilizer, and nonpolar molecular chains of the BR. The BR molecules can inter-diffuse into the intergallery space of the layered silicates more readily with the aid of the compatibilizer and result in an intercalated/exfoliated structure. Additionally, these nanocomposites exhibit higher thermal stabilities than those of the neat BR. The relative water vapor permeabilities of the BR nanocomposites containing 10 parts of organosilicate both in the presence and absence of the compatibilizer were reduced to 20% of that of the neat BR.

Acknowledgment

References

[1] K. Yano, A. Usuki, A. Okada, T. Kurauchi, and O. Kamigaito, *J. Polym. Sci. A: Polym. Chem.*, **31**, 2493 (1993).

[2] D. Ratna, O. Becker, R. Krishnamurthy, G. P. Simon, and R. J. Varley, *Polymer*, **44**, 7449 (2003).

[3] N. Salahuddin, A. Moet, A. Hiltner, and E. Baer, *Eur. Polym. J.*, **38**, 1477 (2002).

[4] J. Fröhlich, R. Thomann, and R. Mülhaupt, *Macromolecules*, **36**, 7205 (2003).

[5] A. Mousa and J. Karger-Kocsis, *Macromol. Mater. Eng.*, **286**, 260 (2001).

[6] Z. Wang and T. J. Pinnavaia, *Chem. Mater.*, **10**, 1820 (1998).

[7] T. K. Chen, Y. I. Tien, and K. H. Wei, *Polymer*, **41**, 1345 (2000).

[8] H. L. Tyan, C. M. Leu, and K. H. Wei, *Chem. Mater.*, **13**, 222 (2001).

[9] S Varghese, J. Karger-Kocsis, and K. G. Gato, *Polymer*, **44**, 3977 (2003).

[10] J. Ma, J. Xu, J. J. Ren, Z. Z. Yu, and Y. W. Mai, *Polymer*, **44**, 4619 (2003).

[11] H. Zhao and D. A. Shipp, *Chem. Mater.*, **15**, 2693 (2003).

[12] H. L.Tyan, K. H. Wei, and T. E. Hsieh, *J. Polym. Sci., Part B: Polym. Phys.*, **38**, 2873 (2000).

[13] Y. I. Tien and K. H. Wei, *Macromolecules*, **34**, 9045 (2001).

[14] Z. Wang and T. J. Pinnavaia, *Chem. Mater.*, **10**, 3769 (1998).

[15] M. Ganter, W. Gronski, H. Semke, T. Zilg, C. Thomann, and R. Mülhaupt, *Kautsch. Gummi Kunstst.*, **54**, 166 (2001).

[16] S. Joly, G. Garnaud, R. Ollitrault, and L. Bokobza, *Chem. Mater.*, **14**, 4202 (2002).

[17] M Krook, A. C. Albertsson, U. W. Gedde, and M. S. Hedenqvist, *Polym. Eng. Sci.*, **42**, 1238 (2002).

[18] R. A. Vaia, H. Ishii, and E. P. Giannelis, *Chem. Mater.*, **5,** 1694 (1993).

[19] W. G. Hwang, K. H. Wei, and C. M. Wu, *Polymer*, **45**, 5729 (2004).

[20] Y. P. Wu, L. Q. Zhang, Y. Q. Wang, Y. Liang, and D. S. Yu, *J. Appl. Polym Sci.*, **82**, 2842 (2001).

[21] M Janis, D, C. Brown, and R. A. Vaia, *Chem. Mater.*, **12,** 3376 (2000).

[22] C. S. Triantafillidis, P. C. LeBaron, and T. J. Pinnavaia, *Chem. Mater.*, **14,** 4088 (2002).

[23] T. Agag, T. Koga, and T. Takeichi, *Polymer*, **42,** 3399 (2001).

[24] J. H. Park and S. C. Jana, *Macromolecules*, **36,** 2758 (2003).

[25] R. Fayt, R. Jérôme, and P. Teyssié, *J. Polym. Sci., Part B: Polym. Phys.*, **27,** 775 (1989).

[26] T. H. Chen, J. J. Zhu, B. H. Li, Z. Y. Yuan, P. C. Sun, Q. H. Jin, D. T. Ding, and A. C. Shi, Chinese patent ZL 02149126.7. (2004)

[27] C. Laurens. C. Creton, and L. Léger, *Macromolecules*, **37**, 6814 (2004).

[28] M. Pluta, *Polymer*, **45**, 8239 (2004).

[29] B. Yalcin and M. Cakmak, *Polymer*, **45**, 6623 (2004).

[30] T. H. Chen, J. J. Zhu, B. H. Li, S. Y. Guo, Z. Y. Yuan, P. C. Sun, D. T. Ding, and A. C. Shi, Macromolecules, **38**, 4030 (2005).

[31] W. G. Hwang, K. H. Wei, and C. M. Wu, *Polym. Eng. Sci.*, **44**, 2117 (2004).

[32] M. Arroyo, M. López-Manchado, and B. Herrero, *Polymer*, **44**, 2447 (2003).

[33] J. Karger-Kocsis and C. M. Wu, *Polym. Eng. Sci.*, **44**, 1083 (2004).

[34] H. R. Dennis, D. L. Hunter, D. Chang, S. Kim, J. L. White, J. W. Cho, and D. R. Paul, *Polymer*, **42**, 9513 (2001).

[35] M. Song, C. W. Wang, J. Jin, A. Ansarifar, Z. Y. Zhang, and M. Richardson, *Polym. Int.*, **54**, 560 (2005).

[36] L. H. Sperling, *Introduction to Physical Polymer Science*, 2nd Edn., John Wiley & Sons, New York (1993), Ch. 9, p. 382.

[37] C. I. Park, O. O. Park, J. G. Lim, and H. J. Kim, *Polymer*, **42**, 7465 (2001).

[38] Y. S. Choi, M. H. Choi, K. H. Wang, S. O. Kim, Y. K. Kim, and I. J. Chung,

Macromolecules, **34**, 8978 (2001).

[39] J. T. Kim, T. S. Oh, and D. H. Lee, *Polym. Int.*, **52**, 1203 (2003).

Table 4A-1 : Formulation of BR/organosilicate nanocomposites.

Material	phr
BR, Taipol 0150	100
Organosilicate, Nanomer I.28E	0-10 (various)
CTB	0–3
CTBN	0 or 3
ZnO	5
Stearic acid	2
Process aid	3.7
Sulfur	1.5
Accelerators	1.5

phr: parts per hundred rubber

Table 4A-2 : Representative vulcanization characteristics of BR/organosilicate nanocomposites.

BR-(I.28E)-(ratio of CTB to I.28E)	t_2 (s)	t_{90} (s)	M_L (lb-in)	M_H (lb-in)	$M_H - M_L$ (lb-in)
Neat BR	169	285	0.76	7.80	7.04
BR-10	81	160	0.89	8.10	7.21
BR-10-7.5	81	168	0.86	7.88	7.02
BR-10-15	82	168	0.81	7.70	6.89
BR-10-30	85	175	0.76	7.30	6.54
BR-10-45	84	175	0.72	6.77	6.05

t_2: Initial scorch time to 2 units of torque increase above minimum torque.

t_{90}: Cure time to 90% of maximum torque development.

M_L: Minimum torque.

M_H: Maximum equilibrium torque.

$M_H - M_L$: Torque increase.

Table 4A-3 : X-Ray diffraction data of BR/organosilicate nanocomposites.

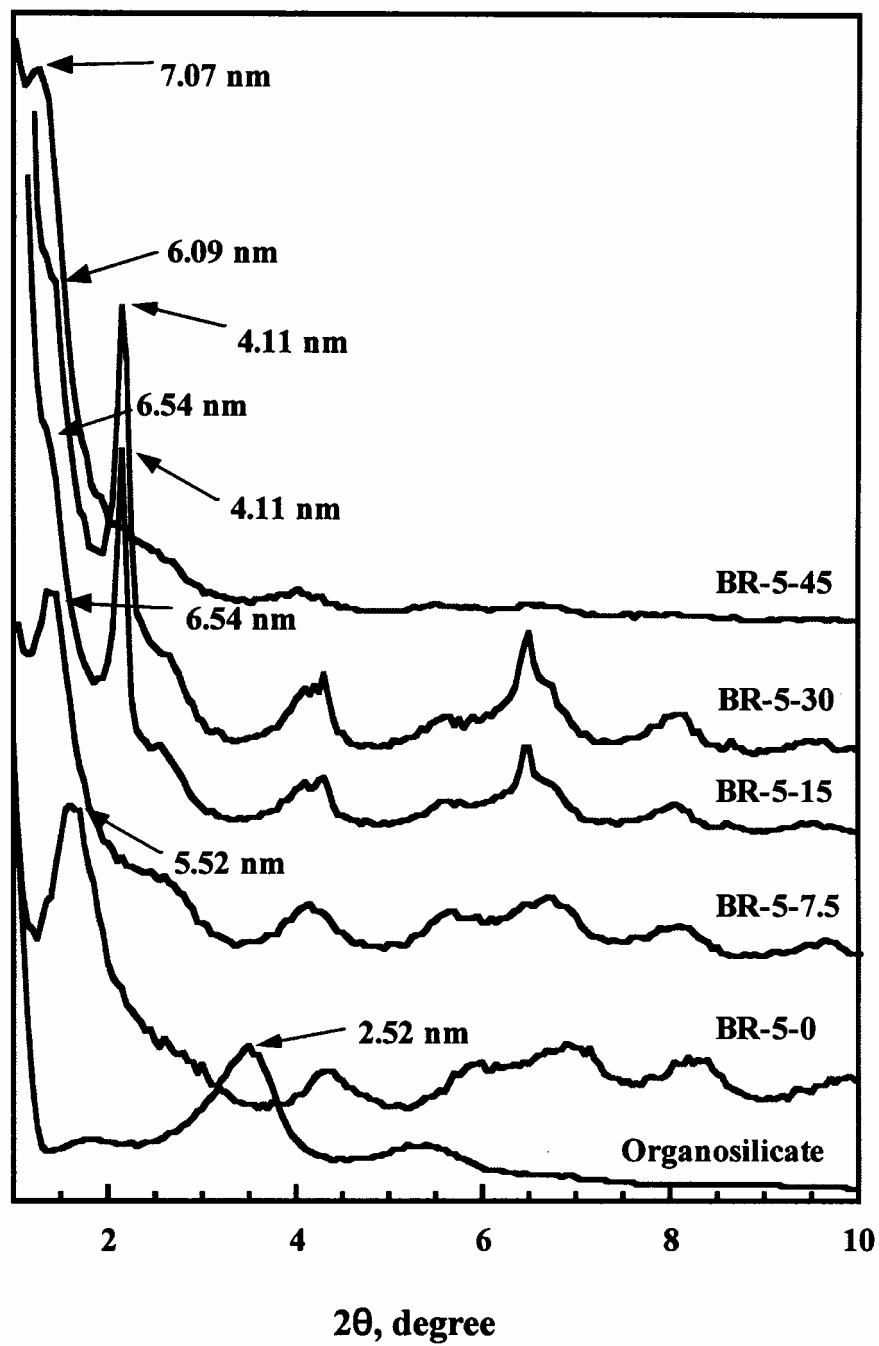| BR-(I.28E)-(weight ratio of CTB to I.28E)	001, A (nm)	001, B (nm)	002, B (nm)
Pure organosilicate	2.52	1.63	
BR-5	5.52	4.03	2.03
BR-5-7.5	6.54	4.17	2.16
BR-5-15	6.54	4.11	2.05
BR-5-30	6.09	4.11	2.05
BR-5-45	7.07	4.21	2.21
BR-7.5	6.09	4.02	2.08
BR-7.5-7.5	6.54	4.19	2.15
BR-7.5-15	6.31	4.01	2.08
BR-7.5-30	6.54	4.01	2.08
BR-7.5-45	6.54	4.21	2.15
BR-10	4.77	4.01	1.98
BR-10-7.5	5.70	4.15	2.13
BR-10-15	5.35	4.07	2.10
BR-10-30	5.89	4.11	2.08
BR-10-45	no peak	–	–

Figure 4A-1. X-ray diffraction patterns of BR nanocomposites containing

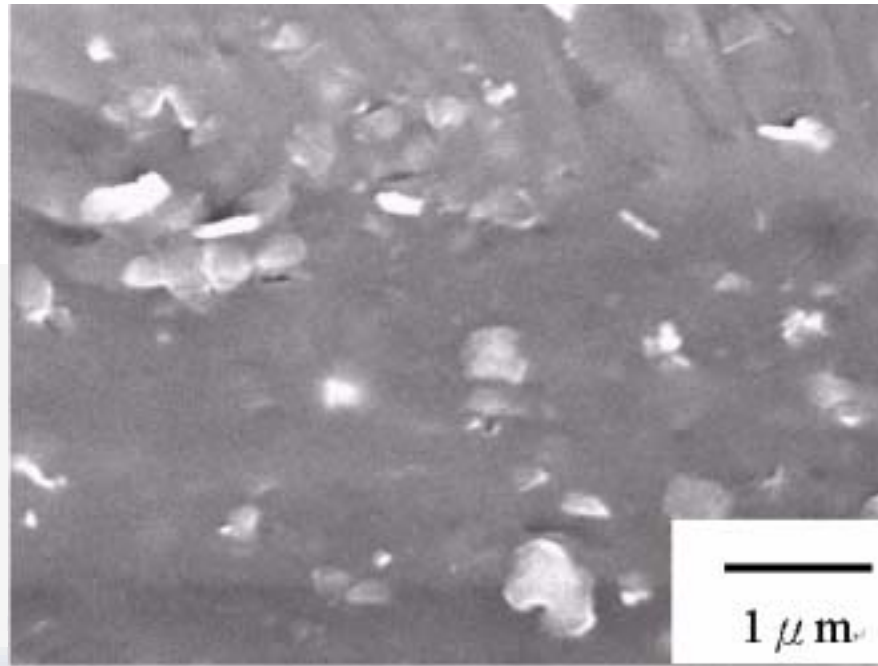various contents of organosilicates.
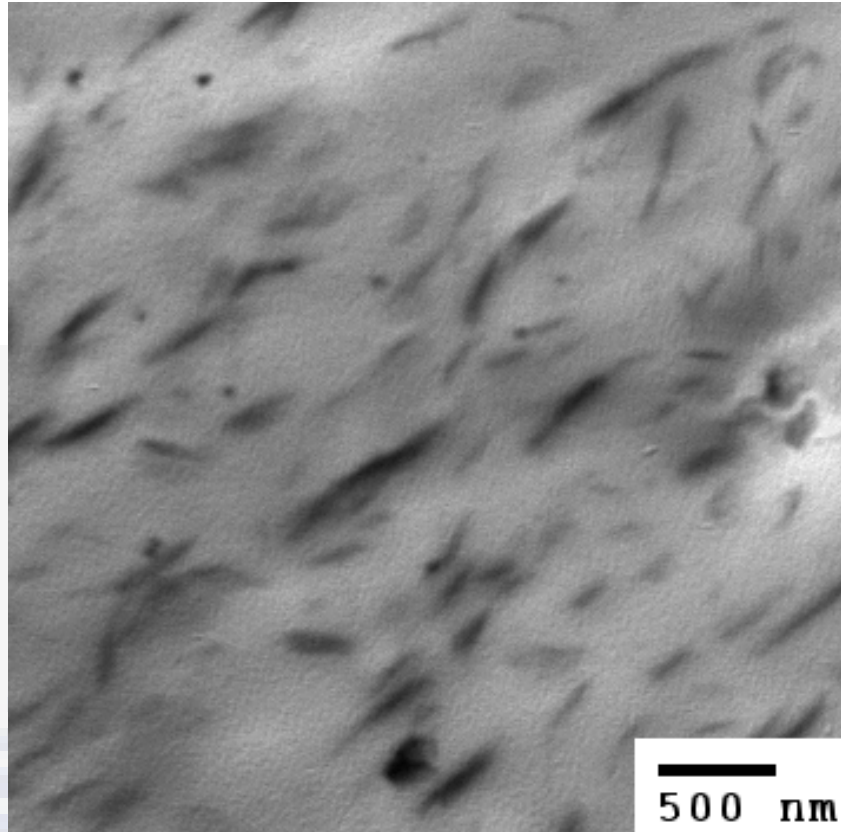
Figure 4A-2. TEM image of the BR nanocomposite containing

10 phr organosilicate and 3 phr CTB.
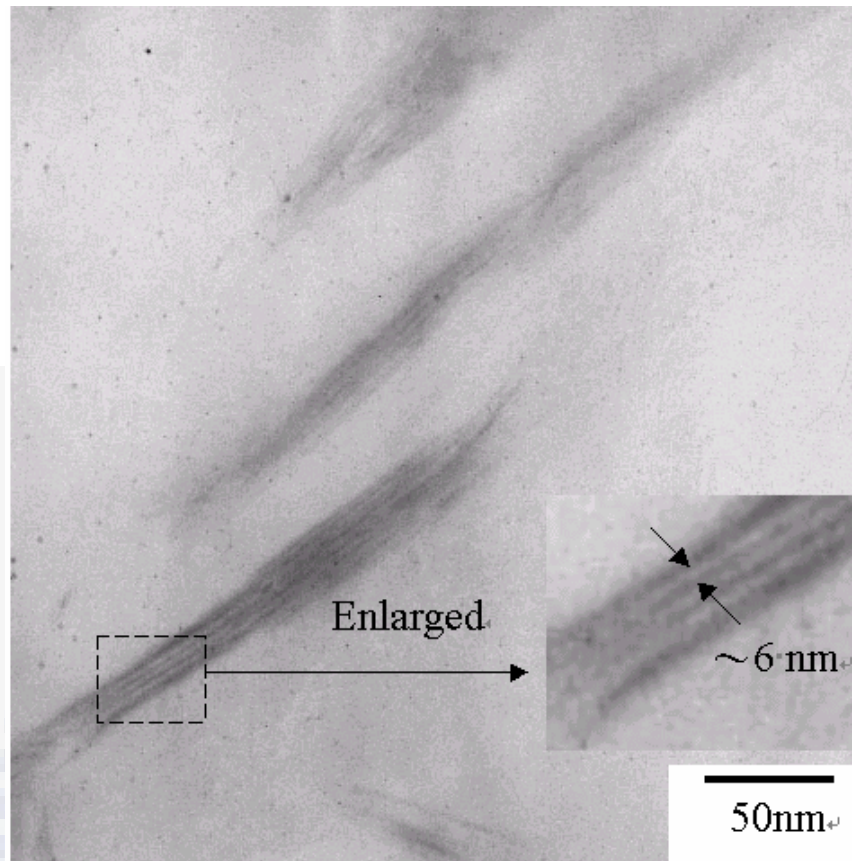
Figure 4A-3. Locally enlarged TEM image of the BR nanocomposite

containing 10 phr organosilicate and 3 phr CTB.
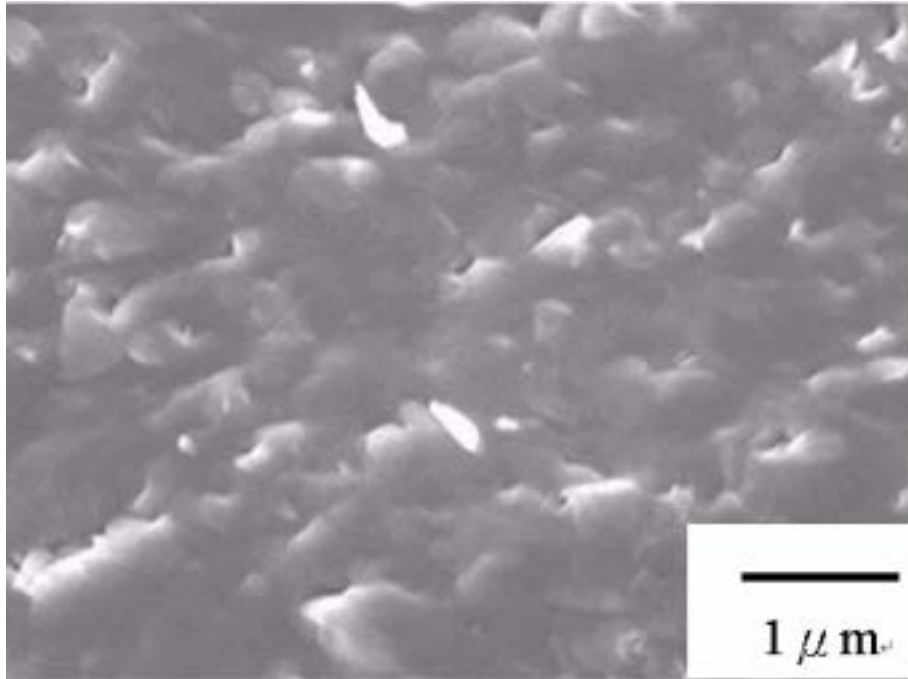
Figure 4A-4. FE-SEM image of the BR nanocomposite containing

10 phr organosilicate and 3 phr CTB.

Figure 4A-5. FE-SEM image of the BR nanocomposite containing
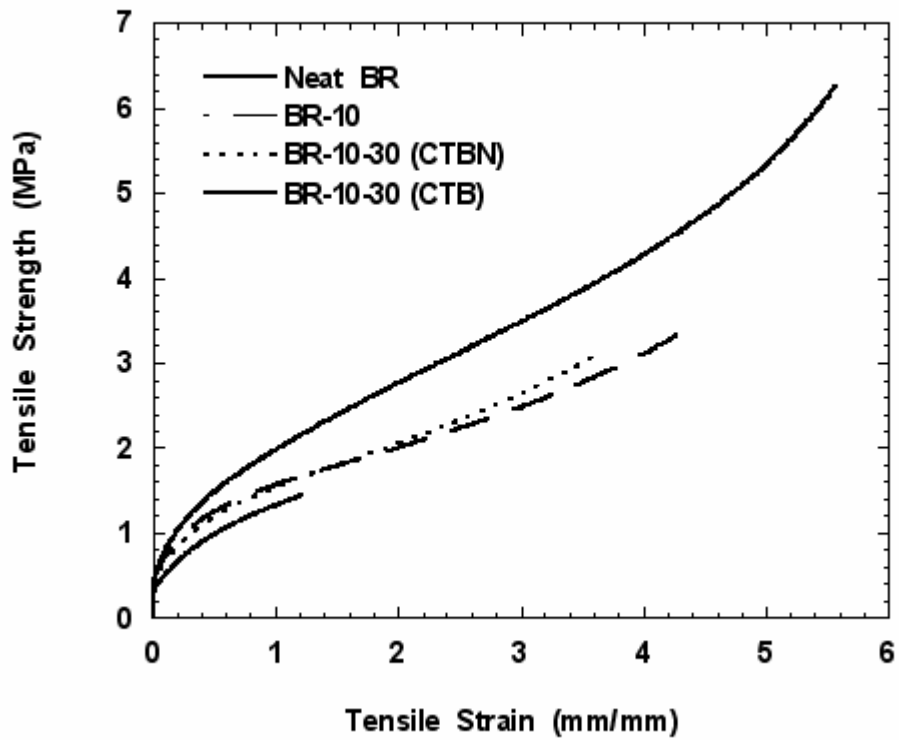
10 phr organosilicate (without CTB).

Table 4B-1 : Crosslinking densities and thermodynamic characteristics of
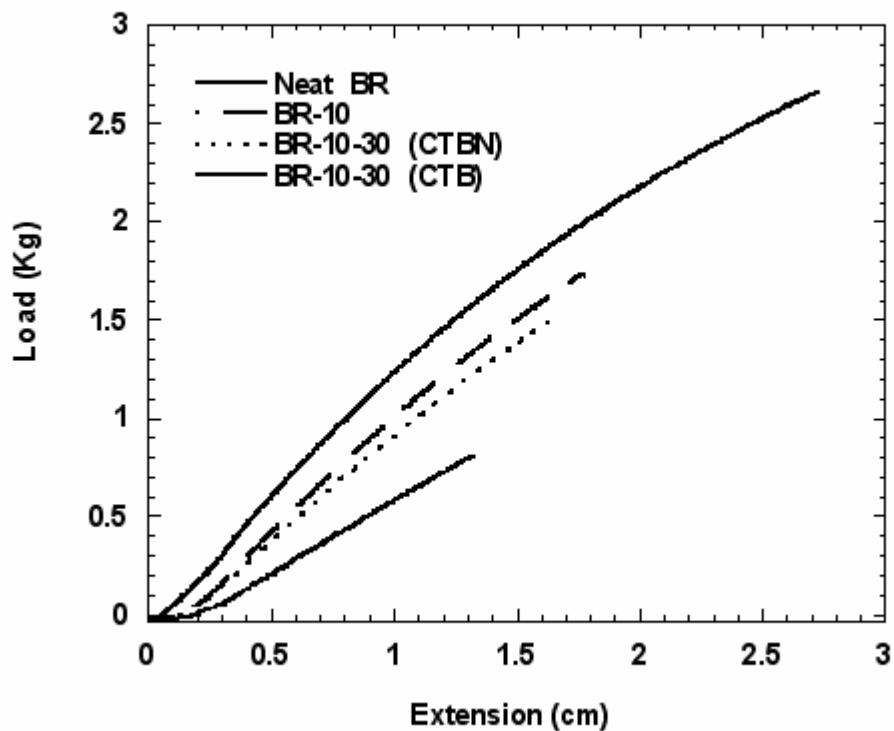BR/organosilicate nanocomposites.

sample	Volume fraction	Crosslink density $(\times 10^{-4}\,\text{mol}\cdot\text{cm}^{-3})$	G $(\text{J}\cdot\text{mol}^{-1})$	S $(\text{J}\cdot\text{mol}^{-1}\cdot\text{K}^{-1})$
Neat BR	0.2025	1.152	-14.96	0.0494
BR-10	0.2010	1.131	-14.68	0.0484
BR-10-7.5	0.2094	1.250	-16.35	0.0540
BR-10-15	0.2080	1.230	-16.05	0.0530
BR-10-30	0.2067	1.210	-15.80	0.0521

**Table 4B-2 :** Thermal properties of BR/organosilicate nanocomposites.

| Sample	Td (°C) at 5% weight loss	Td (°C) at 50% weight loss	E´ $(\times 10^9\,\text{Pa})$	Tg (°C)	tan δ (E´´/E´)
Neat BR	426	510	0.073	−72	1.018
BR-7.5	359	557	0.359	−80	0.475
BR-10	394	561	1.530	−80	0.202
BR-10-7.5	406	522	2.330	−68	0.249
BR-10-15	406	523	2.227	−71	0.258
BR-10-30	409	519	1.961	−70	0.196

Figure 4B-1. Typical tensile stress–strain curves of the BR

nanocomposites containing 10 phr organosilicate in

the presence and absence of compatibilizer.

Figure 4B-2. Typical tear strength curves of the BR nanocomposite

containing 10 phr organosilicate in the presence and

absence of compatibilizer.
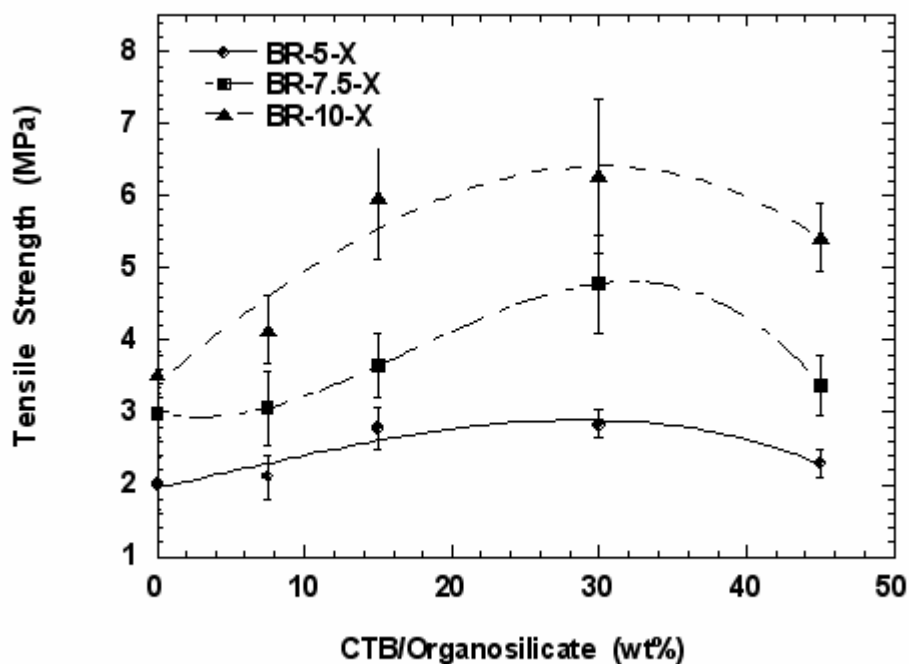
Figure 4B-3. The synergistic effect of the CTB/organosilicate ratio on the

tensile stress–strain curves of the BR nanocomposites

containing various organosilicate contents (neat BR has a

tensile strength of 201 ± 14 Psi).
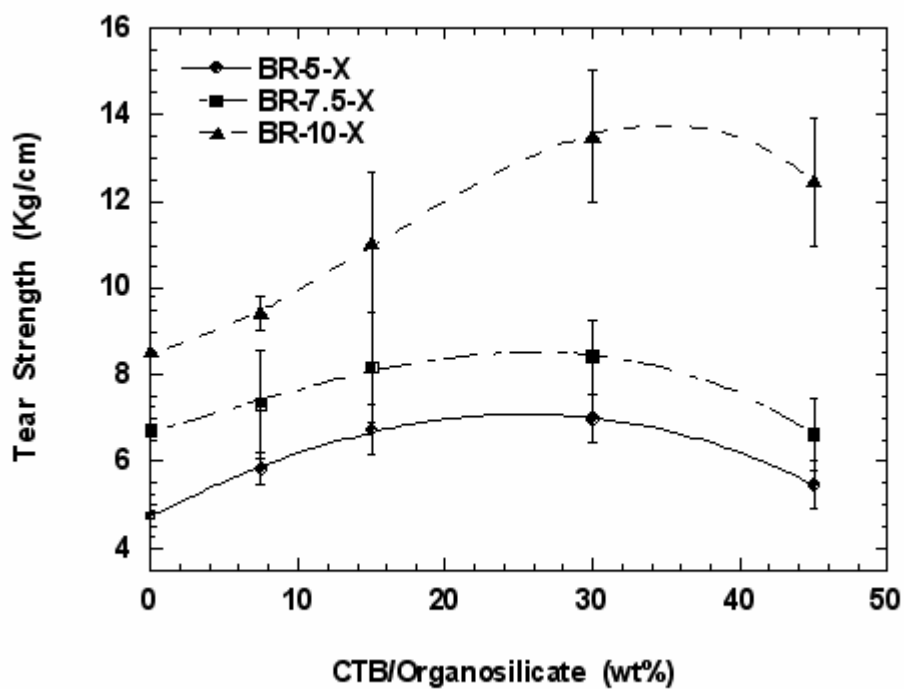
Figure 4B-4. The synergistic effect of the CTB/organosilicate ratio on
the tear strength of the BR nanocomposites containing
various organosilicate contents (neat BR has a tear strength
of 22.83 ± 0.85 lb/in).
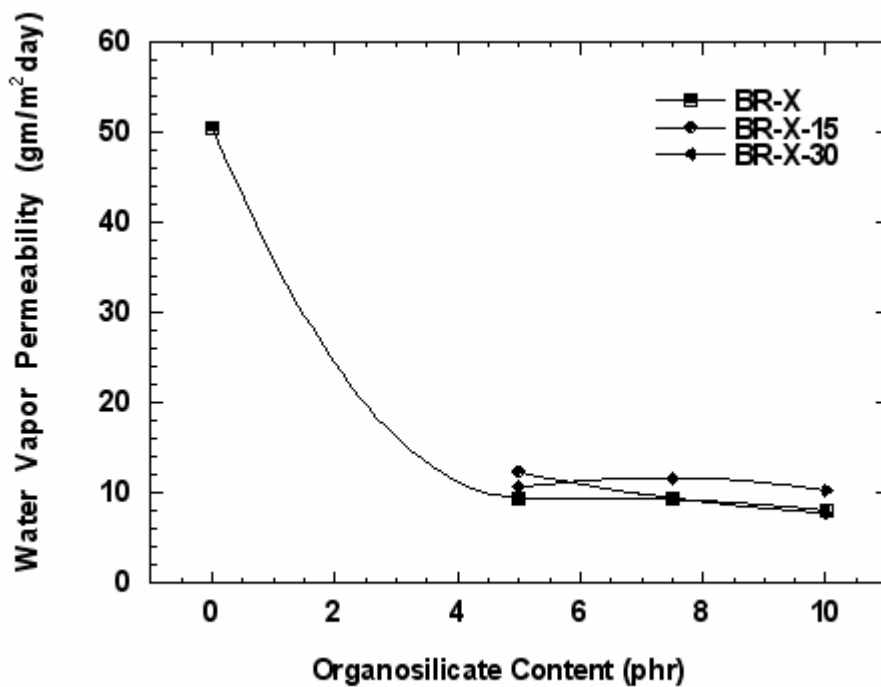
Figure 4B-5. Water vapor permeabilities of the BR nanocomposites

containing various organosilicate contents.

Chapter 5: Conclusions

In the elastomer/layered silicate nanocomposite system, both inorganic and organo-modified nanosilicates with proper selection can be easily dispersed into a polar or nonpolar elastomer matrix through proper process design and form an intercalated and/or exfoliated polymer nanocomposite that having highly improved mechanical, thermal, and barrier properties in each case of the prepared samples. In this thesis, we had successfully applied three different methods to prepared such an elastomer nanocomposite, including latex blending, solvent and elastomer solution, and modified melt intercalation methods, respectively.

In the case of latex blending process, NBR/silicate nanocomposites, with a mostly exfoliated and partially intercalated coexisting structure, were successfully prepared by ball milling of surfactant-treated layered silicates in emulsified solution, followed by latex shear blending. The tensile mechanical properties and tear strengths of these nanocomposites increase with the amount of layered silicates, as compared to that of neat NBR. Additionally, these nanocomposites display higher thermal stabilities than neat rubber.

In the case of solution blending process, NBR/organosilicate nanocomposites, with exfoliated and intercalated structures, were successfully prepared by using polar NBR and layered organosilicate dissolved in a polar solvent directly, and following by a high shear blending method. The hardness, tensile properties and tear strength of these nanocomposites increase substantially with the amount of incorporated organosilicates by containing a few weight percent of layered silicates, as compared to neat NBR. This reinforcing effect can be attributed to strong interactions between the intercalated NBR molecular chains and organosilicate

layers.   Additionally, these nanocomposites exhibit higher thermal stabilities than those of pure NBR.   The relative vapor permeability of nanocomposites containing ten parts of layered silicates is reduced by 85% and 42% for water and for methanol, respectively, as compared to pure NBR.

In the case of melt intercalation methods, we have successfully prepared BR/organosilicate nanocomposites that have intercalated and partially exfoliated structures by using a two-stage melt blending method.   As a result of counteracting the polarity effect and compatibility effect, the tensile properties and tear strengths of these nanocomposites increase substantially—relative to those of the neat BR—upon increasing the amounts of incorporated compatibilizer and organosilicates that contain a low weight percent of layered silicates.   These results are attributed to the significantly improved compatibility and the strong interactions among the polar layered silicates, compatibilizer, and nonpolar molecular chains of the BR.   The BR molecules can inter-diffuse into the intergallery space of the layered silicates more readily with the aid of the compatibilizer and result in an intercalated/exfoliated structure.   Additionally, these nanocomposites exhibit higher thermal stabilities than those of the neat BR.   The relative water vapor permeabilities of the BR nanocomposites containing 10 parts of organosilicate both in the presence and absence of the compatibilizer were reduced to 20% of that of the neat BR.

Besides, based on the experimental results in our laboratory (haven't been submitted), we have also successfully prepared NBR/organosilicate nanocomposites that have intercalated and partially exfoliated structures by using the two-stage melt blending method, directly.   These nanocomposites having outstanding mechanical, thermal, and barrier properties were prepared by melt intercalation method without the help of compatibilizer, which is due to the polar effect and the strong interactions

between the layered silicates and the molecular chains of NBR.

Publication Lists

1. W. G. Hwang, K. H. Wei, and C. M.Wu, "Mechanical, Thermal, and Barrier Properties of NBR/Organosilicate Nanocomposites", *Polym. Eng. Sci.*, **44**, 2117 (2004).

2. W. G. Hwang, K. H. Wei, and C. M. Wu, " Preparation and Mechanical Properties of Nitrile Butadiene Rubber/Silicate Nanocomposites", *Polymer*, **45**, 5729 (2004).

3. W. G. Hwang, K. H. Wei, and C. M.Wu, "Synergistic Effect of Compatibilizer in Organo-modified Layered Silicate Reinforced BR Nanocomposites", *Polym. Eng. Sci.*, 2005, accepted.

4. 韋光華、<u>黃為國</u>、吳昌謀、沈賢，" 丙烯晴-丁二烯橡膠/矽酸鹽奈米複合材料的製備與機械特性"， 2004 年奈米國家型科技計畫成果發表會

5. <u>黃為國</u>、吳昌謀、田耿彰、呂奇明、韋光華，"NBR/Clay 橡膠奈米複合材料之研究"， 2002 材料學會年會.

6. <u>黃為國</u>、吳昌謀、呂奇明、王世松、李昌崙、韋光華，"架橋系統對 EPDM/黏土奈米複合材料之效應"， 2002 材料學會年會.

7. 吳昌謀、<u>黃為國</u>、韋光華，"聚丁二烯/矽酸鹽奈米橡膠之研究"， 2005 高分子研討會年會.

Patent Lists

1. Yu-Hwey Chuang, **<u>Wei-Gwo Hwang</u>**, Ken-Chang Tien, Chang-Mou Wu, Shyan Bob Shen, and Kung-Hwa Wei, "Elastomer nanocomposite and method of preparing the same.", 美國發明專利，申請號：10/905112，申請日：12/16/2004.

<div align="center">

學經歷資料

</div>

- 姓名：黃為國
- 性別：男
- 生日：44 年 04 月 23 日
- E-mail address：jo622@ms52.hinet.net
- Tel：(家) 04-23105956 (手機) 0928-296292
- 聯絡地址：台中市 407 大洲街 107 巷 10 號

學歷

博士候選人：國立交通大學材料科學與工程研究所	2001. 9 ~ present
碩士：國立清華大學高分子研究所	1982. 9 ~ 1985. 6
大學: 國立中央大學化工系	1974.9~ 1978. 6

參與計畫

- 經濟部科專-阻斷型奈米彈性體材料技術等高分子奈米複合材料。
- 經濟部科專-輕量化奈米消能元件技術開發　　。
- 經濟部科專-關鍵元件技術開發-奈米流體阻尼器技術開發。
- 彈性體隔減震技術與元件開發及彈性體/鋼板或纖維複合墊之配方、製程、表面處理技術開發、製備與性能分析。

專長

- 奈米彈性體材料與分散技術：
  1. 層狀矽酸鹽/彈性體奈米複材之製程、特性、界面改質分散技術，包括乳膠摻合、溶液摻合與熔融摻合製程。
  2. 彈性體/纖維組合件之電漿表面處理與接著技術及特性開發。
- 彈性體隔減震相關技術與元件開發。
- 高性能橡膠配方設計、整廠製程設計輸出與規範認證技術。